Design of lanthanide based metal–organic polyhedral cages for application in catalysis, sensing, separation and magnetism

Bell, Daniel; Natrajan, Louise S.; Riddell, Imogen A.

DOI:
10.1016/j.ccr.2022.214786

Document Version
Publisher's PDF, also known as Version of record

Citation for published version (Harvard):
Bell, D, Natrajan, LS & Riddell, IA 2022, 'Design of lanthanide based metal–organic polyhedral cages for application in catalysis, sensing, separation and magnetism', *Coordination Chemistry Reviews*, vol. 472, 214786. https://doi.org/10.1016/j.ccr.2022.214786

Coordination Chemistry Reviews 472 (2022) 214786

Contents lists available at ScienceDirect

Coordination Chemistry Reviews

journal homepage: www.elsevier.com/locate/ccr

Review

Design of lanthanide based metal–organic polyhedral cages for application in catalysis, sensing, separation and magnetism

Daniel J. Bell, Louise S. Natrajan *, Imogen A. Riddell *

Department of Chemistry, University of Manchester, Oxford Road, Manchester M13 9PL, UK

ARTICLE INFO

Article history:
Received 31 May 2022
Accepted 14 August 2022
Available online 6 September 2022

Keywords:
Supramolecular cage
Lanthanide
Self-assembly
Host–guest
Imaging

ABSTRACT

Lanthanide organic polyhedral cage complexes are a class of supramolecular compounds that present exciting opportunities in applications ranging from sensing to catalysis and magnetism. Metal organic polyhedra incorporating transition metal vertices bridged by organic ligands have been extensively studied. By contrast analogous lanthanide complexes, which present additional benefits beyond those of their transition metal counterparts, remain an underrepresented class of supramolecule. One unique property of lanthanide organic cages is the luminescence properties bestowed by the metal ions which offer interesting opportunities in imaging applications, whilst the large ionic radii of the trivalent ions enables the formation of novel structures with opportunities to incorporate ancillary ligands not possible for transition metal structures. This review summarizes the key developments in synthesis and characterization of lanthanide metal organic cages, allowing general structural trends to emerge and highlights the exciting applications already demonstrated for these complexes.

Contents

* Corresponding authors.
E-mail addresses: louise.natrajan@manchester.ac.uk (L.S. Natrajan), imogen.riddell@manchester.ac.uk (I.A. Riddell).

https://doi.org/10.1016/j.ccr.2022.214786
0010-8545/

1. Introduction

In the three and a half decades since metal–organic polyhedra were initially described [1] a series of increasingly complexed architectures have been reported including tetrahedral [2–4], cubic [5–8] and spherical structures [9–11]. These three-dimensional multi-nuclear structures are constructed from multitopic ligands bridging metal ion vertices. The well-defined coordination geometries of transition metal ions [12] and the relatively strong metal to ligand bonding exhibited by these complexes has facilitated the rational design of a myriad of structures [13,14]. By contrast, reports of metal organic polyhedra incorporating lanthanide ions have, until recently, remained sparse [15].

The major challenges associated with development of lanthanide organic polyhedral (LOP) arise from the contracted nature of the 4f valence electrons and the propensity of lanthanide ions to exist in the + III oxidation state which means it is difficult to discriminate one from another chemically. Crystal field effects in lanthanide ions are over three orders of magnitude weaker than for transition metal ions due to effective shielding of the 5s, 5p and 6s electrons [16]. Thus the major discriminating factor between lanthanide ions is their trivalent ionic radii, which for 8 coordinate lanthanides range from lutetium (97.7 pm) to lanthanum (116.0 pm) [17]. The coordination geometries adopted by lanthanide ions are also similar, with a nine coordinate tricapped trigonal prismatic geometry being the most common in lanthanide supramolecular chemistry [18], although lanthanide ion coordination numbers can vary from six up to twelve [19]. Table 1 summarizes and compares the key properties of transition metal ions and lanthanides relevant to their incorporation in polyhedral cage complexes.

A key advantage that lanthanide ions possess over many transition metal ions is atom-like and long-lived luminescence. Both transition metal and lanthanide ions can absorb energy, exciting electrons into higher energy states. Intra 4f-f transitions yield sharp signals, at largely constant, characteristic wavelengths for each lanthanide ion. Compared to organic luminescence, lanthanide signals are generally weaker but possess much longer lifetimes (up to milliseconds), which allows lanthanide luminescence to be time-gated, resulting in the removal of faster, more intense overlapping organic luminescence peaks [20]. The potential for lanthanide complexes in cellular imaging is well recognized [21–24], however current studies tend to focus on mononuclear lanthanide complexes. Multinuclear complexes, as described in this review, offer the potential for increased signal intensity and thus sensitivity. Furthermore, void spaces contained within many of these architectures can be used for host–guest chemistry thus opening up drug delivery and selective sensing possibilities, which are less likely with simpler complexes.

Table 1
Comparison of commonly reported transition metal and lanthanide coordination chemistry features found in polyhedra. Cationic radii were determined *via* various methods [17].

	Transition Metal	Lanthanide
Cation Radii / Å	0.40 [Co(IV)] – 1.37 [Au(I)]	0.977 [Lu(III)] – 1.16 [La(III)]
Coordination Geometry	Fixed geometries governed by crystal field effects	Sterically determined based on cation/ligand size
Oxidation state	Generally + I to + IV	Generally + III
Luminescence	No	Yes
Magnetism	S_{max} = 2.5, d^5	S_{max} = 3.5, f^7
Spin Crossover	Yes	No
Bioavailability	Frequent	Very rare

Lanthanide organic polyhedra (LOP) or cages present exciting opportunities beyond those of their transition metal counterparts, especially with respect to their intrinsic physical properties including luminescence and magnetism. In this review we evaluate advances in ligand design (Section 2) which have supported the development of LOP (Section 3), and discuss the novel applications (Section 4) demonstrated for LOP. With this review, we aim to identify structural features, which will support the continued discovery and development of novel lanthanide polyhedra, as well as highlight future opportunities for this class of molecule. We also include relevant publications on lanthanide helicates (section 3.1.1). Helicates commonly lack internal void space and are not generally defined as polyhedra, however detailed studies into the self-assembly of helicates through kinetic and thermodynamic parameters provides essential insight into lanthanide self-assembly which is relevant to the larger structures targeted in this review. Discussion of lanthanide clusters [25–27], lanthanide coordination polymers [16,28,29] and lanthanide-based knots [30,31] fall outside the scope of this review and these have been reviewed in detail in other works.

2. Evolution of lanthanide binding motifs

Over the past three decades, the number of ligands used in the self-assembly of lanthanide complexes, and the variation in coordination moieties employed has grown considerably. Notably, the increased ionic radii of trivalent lanthanide ions in comparison to their transition metal ion counterparts allows for large ligand coordination numbers (see Table 1). The majority of lanthanide supramolecular structures contain nine-coordinate ions, most commonly arranged in a tricapped trigonal prismatic coordination geometry. To satisfy this nine-coordinate preference, tridentate binding moieties are typically employed, each of which contains three donor groups. Hard donor atoms according to the Pearson classification, frequently nitrogen or oxygen that are complementary to the hard Lewis acidic lanthanide ions, are most utilized.

Initial reports of multinuclear lanthanide structures employed benzimidazole-pyridine-benzimidazole binding sites (Chart 1; **1**) [32]. Though the architectures yielded were stable in acetonitrile luminescence was quenched in the presence of water, suggesting non-optimal ligand wrapping around the lanthanide centers. Conversion of the terminal benzimidazole group to a carboxylic acid increased quantum yields (Chart 1; **2**) [33]. More recent examples have introduced dipicolinamide binding sites (Chart 1; **3**) which dramatically reduced luminescence quenching, suggesting reduced interaction of the metal ion with water molecules through improved shielding of the metal ion by the ligand [34]. Chiral centers have also been installed through functionalization of the terminal amide group on the dipicolinamide moiety, enabling formation of enantiomeric ligand pairs. For reported examples, all stereocentres within a molecule had the same configuration, resulting in (*S,S*)- or (*R,R*)- ditopic ligands, for example. Complexation of enantiomerically pure ligands yielded a single enantiopure species in solution, indicating that ligand enantiomers can direct axial chirality in supramolecular lanthanide architectures. In previous examples complexation of achiral ligands resulted in a racemic mixture of homochiral architectures.

Further alterations to the dipicolinamide binding sites focused on increasing the ligands' ability to sensitize lanthanide luminescence, in turn leading to higher quantum yields. Low quantum yields, below 10 %, are common in the literature and were identified as a factor that could ultimately limit the application of lanthanide architectures. A facile change was to employ strongly absorbing organic moieties, such as chromophores, as substituents on terminal amide groups, with a common example being a naph-

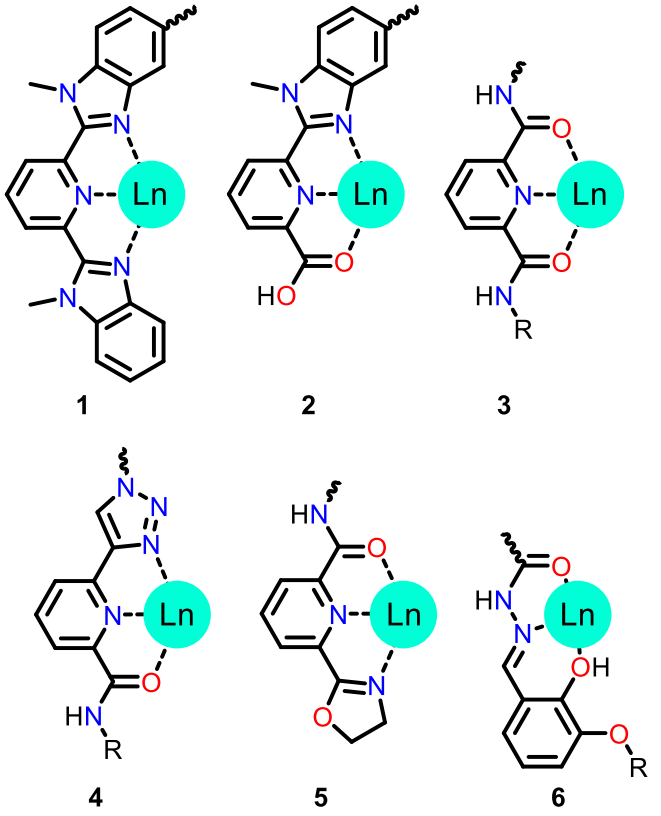

Chart 1. Commonly reported lanthanide coordination sites: 1) benzimidazole-pyridine-benzimidazole; 2) benzimidazole-pyridine carboxylic acid; 3) dipicolinamide; 4) triazole-pyridine-amide; 5)oxazoline-picolinamide; 6) malonohydrazone.

thalene antenna, which strongly absorbs in the 280 nm region. Replacing an amide group with a triazole moiety (Chart 1; **4**) adjacent to the linkers allowed quantum yields above 50 % to be reported. This increased quantum yield was attributed to increased rigidity and conjugation of the ligand, which reduced energy loss to non-radiative pathways [35].

The lack of water-stable species larger than Ln_2L_3 helicates remains a major drawback of lanthanide architectures. In 2017, Sun and coworkers demonstrated that by converting the terminal amide group on the dipicolinamide binding sites to a five-membered oxazoline ring (Chart 1; **5**) Ln_4L_4 tetrahedra that were stable in an acetonitrile solution with up to 10 % water could be prepared. Incorporation of 10 % water within the reaction media represented a significant step forward in the preparation of 'water-proof' lanthanide architectures [35].

Another prominent binding motif in the literature is the malonohydrazone binding site (Chart 1, 6). Larger lanthanide ions bind malonohydrazone moieties in a tridentate fashion (Chart 2, **6A**), accommodating three ligands around a lanthanide center. Duan and coworkers have extensively used malonohydrazone binding sites with Ce(III) ions, yielding Ce_2L_3, Ce_4L_6 and Ce_4L_4 architectures [36,37]. Two alternative malonohydrazone binding modes have also been reported when smaller lanthanide ions (Gd(III) and Dy(III)) were used. The second mode (Chart 2, **6B**) utilizes two phenolic oxygen on the terminal aryl moiety, giving a bidentate site. Finally, a bimetallic mode was reported consisting of bi- and tridentate sites, featuring a μ_2-bridging phenolic oxygen (Chart 2, **6C**). The existence of these alternative binding modes has resulted in unusual architectures, including circular helicates (Ln_4L_4 [38] and Ln_6L_6 [39]) and $Ln_{12}L_{12}$ octahedra [40].

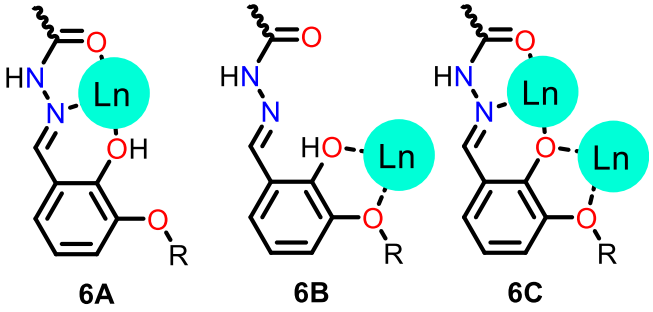

Chart 2. Binding conformations of malonohydrazone moieties: **6A** is the most common tridentate binding mode observed when binding to Ce(III); **6B** is a bidentate binding site; and **6C** is a bimetallic binding mode featuring μ_2-bridging phenolic oxygens as observed in circular helicates [38–40].

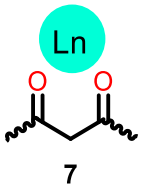

Fig. 1. A bidentate 1,3-diketone binding site (**7**) with a lanthanide ion.

The bidentate 1,3-diketone binding site (Figs. 1, 7) has also seen limited use in the field. Due to the smaller size and reduced denticity of the 1,3-diketone binding moieties, more ligands can bind around a single lanthanide ion leading to the formation of Ln_2L_4 helicates [41]. Further structures have been reported utilizing co-ligands, which provides steric blocking within the lanthanide coordination sphere altering the angles between ligands [42].

3. Self-Assembled multinuclear lanthanide architectures

3.1. Homometallic assemblies

The vast majority of self-assembled lanthanide cages reported incorporate a single species of metal ion. This generally simplifies complex characterization however mixed-metal systems may benefit from incorporation of less labile metal ions, particularly transition metals that are more robust to hydrolysis (see Section 3.2).

3.1.1. Helicates

Supramolecular metal–organic helicates can have varying numbers of metal ions and ligands. Helicates typically lack void pockets and are therefore not considered cage molecules, and do not display cavity based applications such as host–guest derived sensing. Like polyhedra, however, helicates do undergo spontaneous self-assembly, the outcome of which is governed by factors including ligand geometry [43], metal: ligand stoichiometry [38] and the presence of template ions [39]. Previous reviews have discussed self-assembly of lanthanide helicates in depth [44–48]. Here, we provide a brief overview highlighting key representative examples which inform the development of lanthanide cages.

The first report of a dinuclear helicate formed using lanthanide ions was published in 1992 [32]. The triple-stranded $[Eu_2L_3]^{6+}$ complex was generated from a *bis*tridentate ligand (**8**) incorporating coordinating benzimidazole and pyridine moieties. The coordination sphere of the europium(III) ion was thus fulfilled through the binding of three tridentate ligands. This binding site was however prone to hydrolysis and further work has focused on increasing the metal–ligand bond stability (Fig. 2).

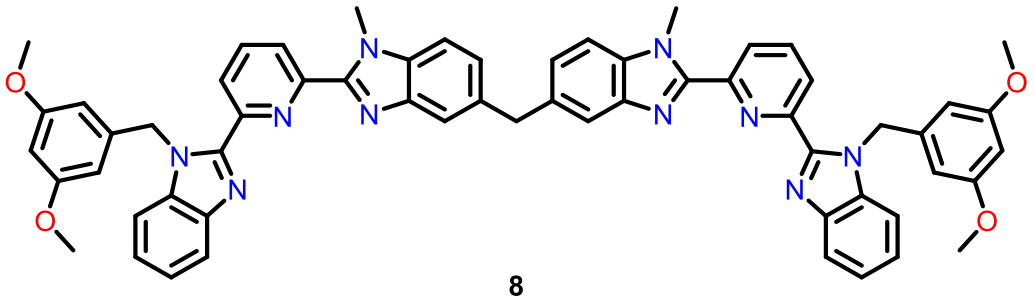

Fig. 2. Benzimidazole-pyridine-benzimidazole-based ligand (**8**) synthesized by Piguet and coworkers, used in the first dinuclear lanthanide helicate [32].

Conversion of the terminal benzimidazole group to a carboxamide group has been shown to increase the $[Eu_2L_3]^{6+}$ complex stability in aqueous environments [33]. Analysis of the single crystal X-ray diffraction data of the lanthanide coordination sites confirms shorter lanthanide-donor bond lengths in the carboxamide moiety compared with the benzimidazole moiety. Shorter lanthanide donor bonds reduce the opportunity for water molecules to directly bind to the metal ion displacing the ligand. Moreover, restricted access of solvent molecules to the europium(III) center also increases the europium luminescence quantum yield through decreased quenching. Further systematic changes to the ligand were performed by converting the carboxamide groups on the ligand to terminal carboxylic acid groups. The helicate formed with this ditopic carboxylic acid ligand($L^{\#}$) was shown to be extremely stable in aqueous solutions having an equilibrium constant of 10^{26} M^{-1} (where the equilibrium measured at pH 7.2, 298 K in H_2O is defined as 2 Eu + 3($L^{\#}$–2H) ⇌ $Eu_2(L^{\#}–2H)_3$ and [$L^{\#}$] = 1.05 × 10^{-5} M, 0 < [Ln] < 1.6 × 10^{-5} M).

Mass spectrometry analysis of solutions containing triple-stranded lanthanide helicates indicate three major species can be present; LnL_2, Ln_2L_2 and Ln_2L_3; although the formation of these species is stoichiometrically (M:L) dependent [49]. Studies indicate that at a 2Ln:3L starting material ratio the Ln_2L_3 helicates are more thermodynamically stable than their Ln_2L_2 counterparts [33,50]. This observation is consistent with the initial observations that ligands that effectively shield lanthanide ions from solvent molecules give rise to more robust structures. These observations led the authors to propose the following four-step process for helicate self-assembly (Fig. 3).

Detailed titration studies investigating the effect of the Ln:L stoichiometry indicated that the double stranded helicate (Ln_2L_2) formed preferentially when the lanthanide was in excess, while the triple stranded helicate (Ln_2L_3) was the major species formed when the ratio of Ln:L was between 0.1 and 0.8. This proposed mechanism was operative regardless of whether the metal ion (Ln) or ligand (L) was in excess; the self-assembly kinetics were however affected [49]. When lanthanide ions were in excess the initial step (i) was an irreversible process with the rate of reaction increasing with total lanthanide concentration. Conversely, the rate of formation of LnL_2 decreased with increasing lanthanide concentration. The rate of the third step (iii), yielding Ln_2L_2, was independent of concentration, which suggested rapid formation of this species. The formation of the bimetallic triple-stranded helicate (Ln_2L_3) was completed with the addition of a third ligand, which was the rate-determining step. By contrast, when excess ligand was present, the first step (i) was found to be reversible, whereas step (ii) was deemed irreversible. The first two steps had a positive linear relationship between ligand concentration and rate constant. The rate constant of step (iii) slowly decreased as ligand concentration increased. An inverse relationship between

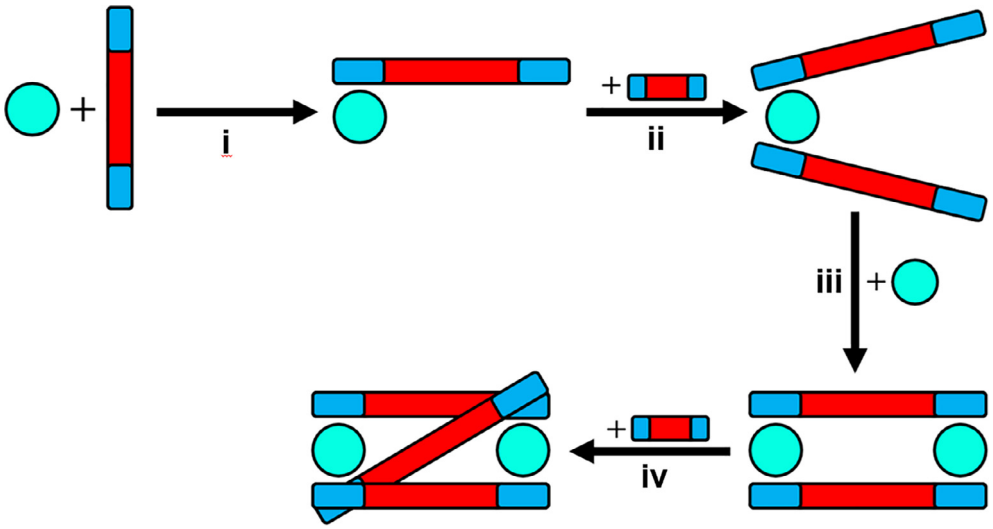

Fig. 3. Proposed mechanism of Ln_2L_3 helicate formation. Cyan spheres = lanthanide ions. Red bars = simplified C_2-symmetric ligands, with binding sites in blue [49]. (For interpretation of the references to colour in this figure legend, the reader is referred to the web version of this article.)

ligand concentration of rate constant was also observed in the final step.

Further systematic studies have investigated the effect of altering the linker bridging between the two tridentate binding groups of ditopic linkers. For all linkers investigated (Figs. 4, 9-11) a Ln_2L_3 stoichiometry was found to generate the most stable complexes [51]. Ligands with bulkier linkers (**11**) were found to have lower association constants than smaller linkers (**9**), this was attributed to the reduced rigidity of these ligands.

Gunnlaugsson and coworkers also employed chiral induction to transfer point chirality on the organic ligand (*R,R* or *S,S*) to the metal centers (ΛΛ or ΔΔ) within the helicate, enabling generation of enantiopure helicates [51]. This strategy was further explored by Guo, Sun and coworkers who employed a chiral ligand incorporating a pyrene linker which gave enantiopure helicates that were differentiated by ^{1}H NMR spectroscopy following the addition of Δ-TRISPHAT (tris(tetrachlorocatecholato)phosphate), due to the formation of diastereomeric ion pairs [52].

Inclusion of additional tridentate binding sites within a linear ligand has been shown to yield longer triple stranded helicates (Fig. 5). Elegant work by Piguet and coworkers synthesized tri-(Ln_3**12**$_3$) [53] and tetranuclear triple stranded helicates (Ln_4**13**$_3$) [54], via the addition of benzimidazole-pyridine-benzimidazole binding sites between terminal benzimidazole-pyridine-amide moieties. As with Ln_2L_3 helicates, formation of the desired architectures was dependent on the stoichiometry of the starting materials. This work has been comprehensively summarized by the authors in reference [53].

Although the vast majority of lanthanide helicates have a Ln_2L_3 composition, a handful of alternative architectures have also been reported including a series of Ln_2L_4 helicates employing bidentate β-1,3-diketone binding sites (Fig. 1). These complexes accommodate four ligands, rather than three, at each lanthanide center [55–58]. Combining the effective lanthanide sensitization properties of the aromatic β-diketonates incorporated within the ligand alongside chiral moieties on the ligand has enabled enantioselec-

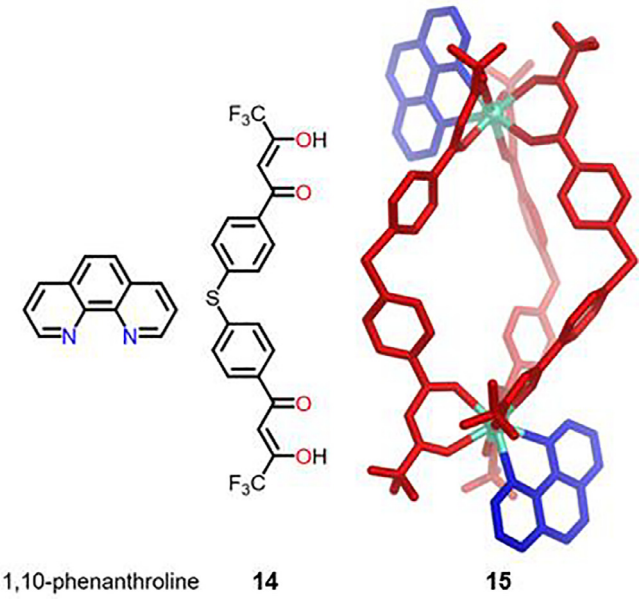

Fig. 6. Structure of a Ln_2(**14**)$_3$(1,10-phenathroline)$_2$ (**15**) architecture synthesized by Li and coworkers (**14** = red; 1,10-phenanthroline = blue) [58]. (For interpretation of the references to colour in this figure legend, the reader is referred to the web version of this article.)

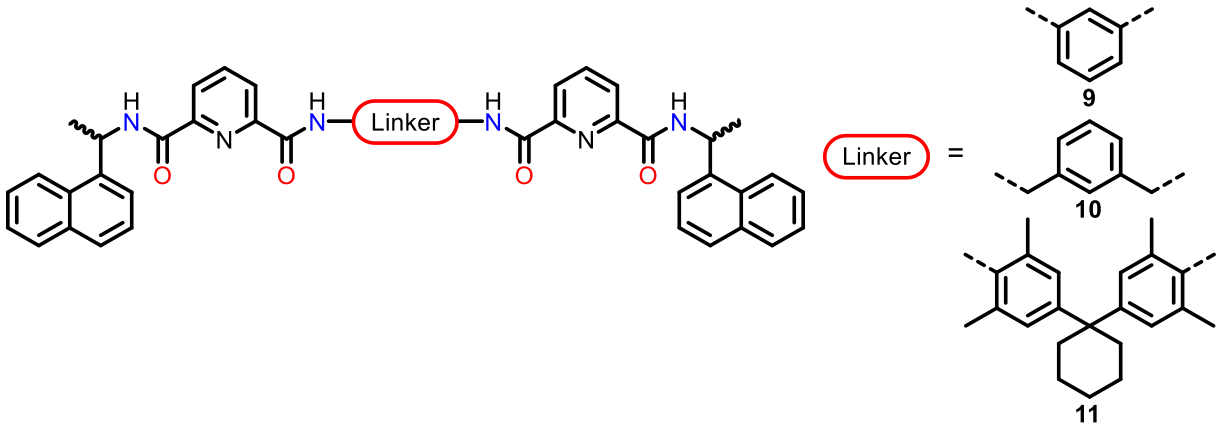

Fig. 4. Picolinamide-based ligands synthesized by Gunnlaugsson and coworkers were used to determine how linker size affects the formation of dinuclear triple stranded helicates. Top (**9**) 1,3-phenyl linker; middle (**10**) 1,3-benzyl linker; bottom (**11**) 4,4′-(cyclohexane-1,1-diyl)bis(1,3-dimethylbenzene) linker [51].

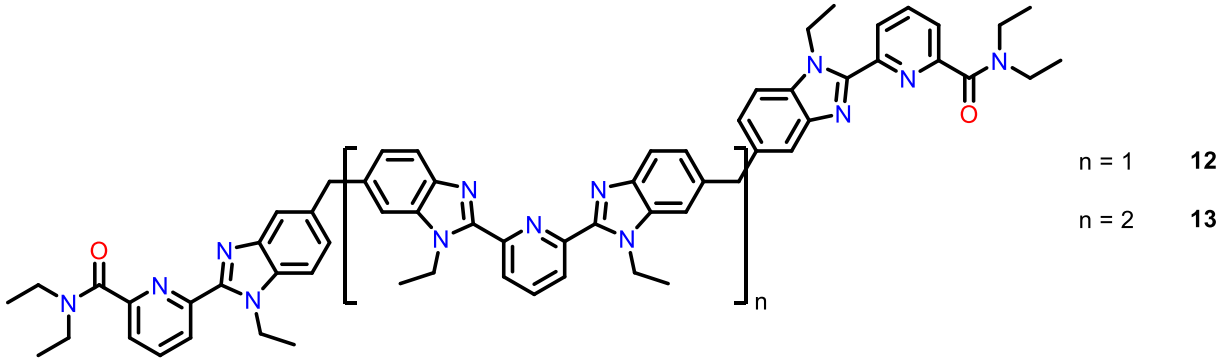

Fig. 5. Two ligands (**12** and **13**) synthesized by Piguet and coworkers which yielded triple-stranded helicates when complexed with Ln(OTf)$_3$ [53,54].

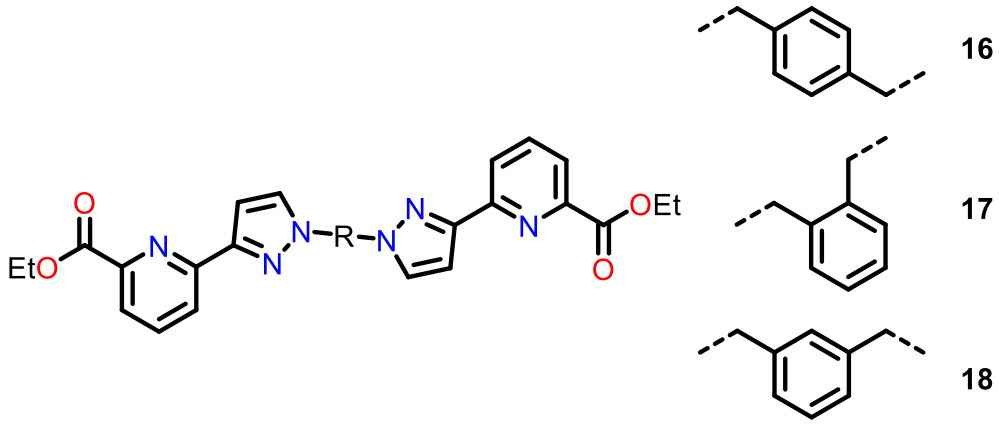

Fig. 7. Three ligands (**16**–**18**) synthesized by Ward and coworkers which yielded a range of small lanthanide architectures [61].

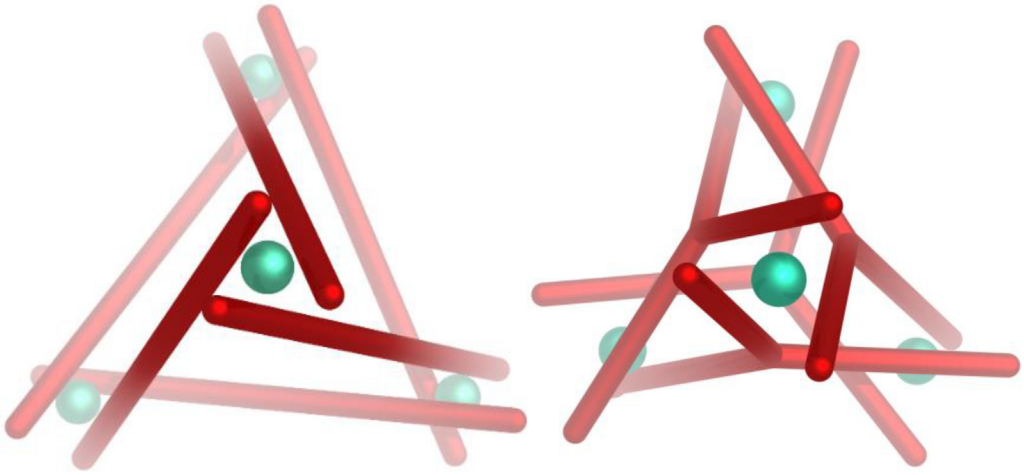

Fig. 8. Schematic diagrams of edge-bridged (left) and face-capped tetrahedra (right). Simplified ligands shown in red, metal ions as green spheres. (For interpretation of the references to colour in this figure legend, the reader is referred to the web version of this article.)

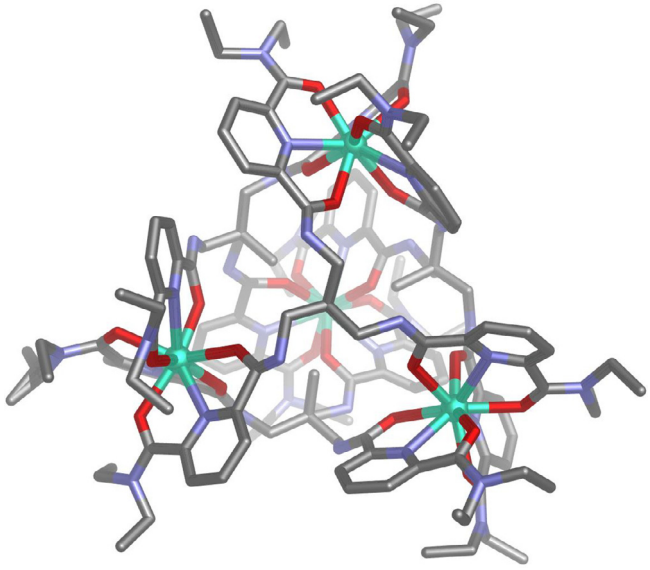

Fig. 9. Crystal structure of the first reported $[Tb_4L_4]^{12+}$ lanthanide architecture (**27**), synthesized by Hamacek and coworkers [64].

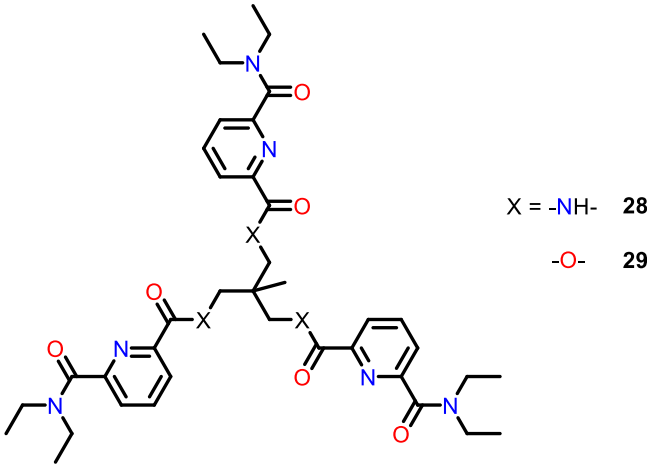

Fig. 10. C_3-symmetric tritopic ligand family synthesized by Hamacek and coworkers, used in the formation of face-capped lanthanide tetrahedra [66,67].

tive formation of helicates displaying intense circularly polarized luminescence and high quantum yields (up to 68 %) [56]. More recently the same group have explored the formation of $M_2L_3(L')_2$

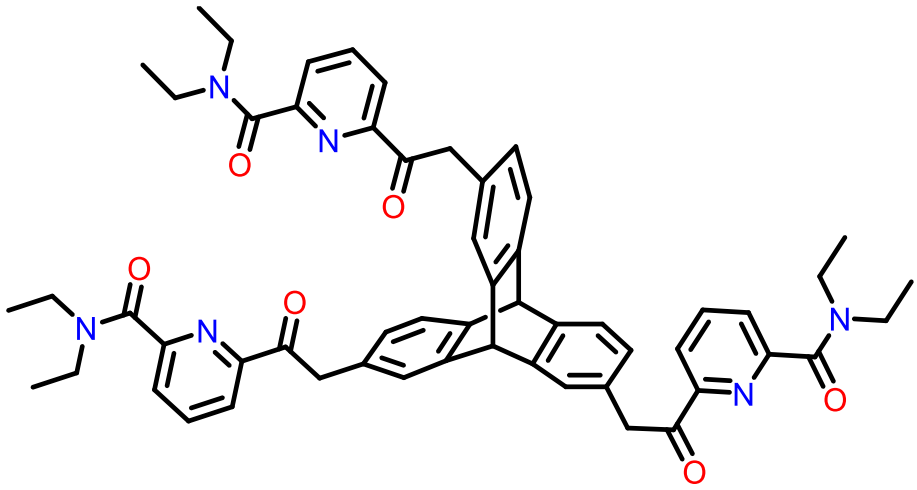

Fig. 11. The C_3-symmetric ligand **30** synthesized by Hamacek and coworkers, employing a central triptycene linker [68].

complexes (Fig. 6) which incorporate three bidentate ligands (**14**) in addition to two ancillary ligands, one associated with each metal center. Incorporating chiral BINAPO (2-diphenylphosphorylk-1-(2-diphenylphosphorylnaphthalen-1-yl)naphthalene) ligands as the ancillary ligands enabled stereoselective control over the self-assembly process in contrast to the incorporation of phenanthroline, which generated a racemic mixture of Δ and Λ helicates (**15**).

A limited number of circular helicate architectures have also been reported, with a varying number of components between Ln_3L_3 [59] to Ln_6L_6 [39,60]. The first lanthanide circular helicate was reported by Piguet and coworkers in 2005 [59]. This trimetallic Ln_3L_3 architecture was observed as a byproduct of Ln_2L_3 formation when using a ligand incorporating a picolinamide-benzimidazole binding site. Isolation of the complex was achieved *via* crystallization, using a 1:1 metal: ligand stoichiometry at high concentrations. Single-crystal X-ray diffraction analysis indicated that triflate counterions, water and acetonitrile solvent molecules saturated the lanthanide coordination sphere. In solution, the Ln_3L_3 architecture was in equilibrium with a bimetallic double-stranded helicate.

Formation of a tetranuclear circular helicate (Nd_4**16**$_4$) from a bitopic ligand **16** has also been reported by Ward and coworkers (Fig. 7) [61]. The lanthanide binding sites in the (Nd_4**16**$_4$) complex are partially saturated with two N,N',O chelating groups whilst water and acetonitrile solvent molecules occupy the remaining ion binding sites (three per metal). Formation of a Nd_2**16**$_3$ helicate with a 2:3 Nd:**16** stoichiometry was also reported. Ln_2L_2 species were observed with **17** and **18**, and in both cases small organic anions were observed to be sandwiched between the bridging ligands [61]. The organic anions were hypothesized to be a result of Ln-catalyzed breakdown of the reaction solvents MeCN and $MeNO_2$

Further stoichiometric dependence was probed by Konar and coworkers, using an ethylene-bridged hydrazone-based ligand (Scheme 1, 19) [38]. In a 1:2 metal: ligand stoichiometry a bimetallic triple-stranded helicate (**20**) formed. However, when a 2:1 metal: ligand stoichiometry was employed, a tetranuclear quadruple-stranded circular helicate (**21**) formed. Both helicates formed as a racemic mixture of Δ and Λ enantiomers. Differences in self-assembled structures could be rationalized by consideration of the three different binding site configurations of the hydrazone group (Fig. 2). When a 1:1 stoichiometry was employed, a tridentate binding mode (Chart 2, 6A) was favored at both binding sites. With more lanthanide ions per ligand, one of the binding sites favored a bimetallic binding site with a μ_2-bridging phenolic oxygen (Chart 2, 6C) which allows for simultaneous bi- and tridentate binding of two lanthanide ions. Due to this bimetallic binding site, the coordination sphere of the lanthanide ions was completed through coordination of a nitrate counterion. Single crystal X-ray diffraction analysis of the structure indicated that a single nitrate ion bound to all four lanthanide centers templates the tetranuclear circular helicate architecture.

The effect of the anion on the multinuclear structures generated with the ethylene-bridged hydrazine-based ligand **19** was probed further by replacement of the nitrate salt with a perchlorate salt. The resulting structure was a Ln_6L_6 circular helicate in which methanol saturated the lanthanide coordination sphere in place of the nitrate counterion observed in complex **21** [39]. A single crystal X-ray structure of **22** showed two perchlorate ions were present inside the structure one above and one below the center of the lanthanide ion plane. Conversion from the Ln_6L_6 helicate (**22**) to the Ln_4L_4 architecture (**21**) occurred upon the addition of nitrate ions. The reverse transformation (**21** → **22**) was not observed following addition of excess perchlorate, suggesting that the nitrate ion coordinates more strongly to the lanthanide metal center. Other species, such as CO_2 and K^+, have been observed to influence the formation of the tetra- and hexanuclear species [62]. Employing a similar ligand, possessing a butylene linker rather than the ethylene linker [40], a comparable Ln_4L_4 circular helicate was observed to form with azide anions in place of nitrate as the template. Furthermore, with the lengthened linker larger architectures were formed when complexed in the presence of hydroxide ions, including a Ln_8L_8 dual triple-stranded helicate and a $Ln_{12}L_{12}$ octahedral, which featured similar binding environments in **20** and **21** [40].

Yuasa and coworkers also reported the synthesis of a tetranuclear circular helicate (Scheme 2), using previously reported 1,3-bis(4,4,4-trifluoro-1,3-dioxobutyl)phenyl (BTP) ligand (**23**), which incorporates bidentate β-1,3-diketone binding sites bridged by a 1,3-phenyl linker [42,56]. A 2:3 metal: ligand stoichiometry yielded a bimetallic triple-stranded helicate structure with three water molecules bound to each lanthanide ion (**24**). A tridentate co-ligand, Ph-Pybox (2,6-bis(4-phenyl-4,5-dihydrooxazol-2-yl)pyridine) (**25**), was introduced at 1:2 BTP: Ph-Pybox stoichiometry in solution, resulting in the formation of a (Ph-Pybox)$_4Ln_4L_6$ architecture (**26**) with Ph-Pybox enantiomers directing helicity. (S)-Ph-Pybox directed (P)-helicity whilst (R)-Ph-Pybox directed (M)-helicity. The square-like Ln_4L_6 core featured two sets of opposing edges. Two of the edges contained two BTP ligands lying above and below the lanthanide plane, with the remaining two edges

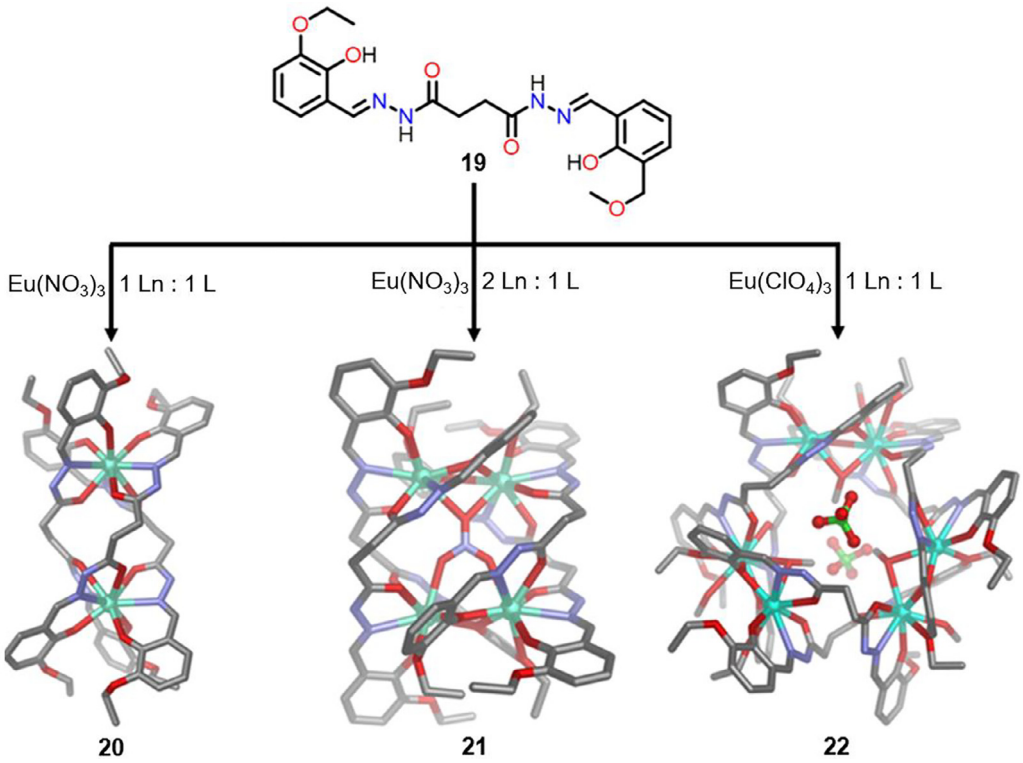

Scheme 1. Malonohydrazone-based ligand (**19**, top) synthesized by Konar and coworkers, with three complexation products (**20**–**22**) formed with nitrate and perchlorate counterions in different stoichiometries [38,39].

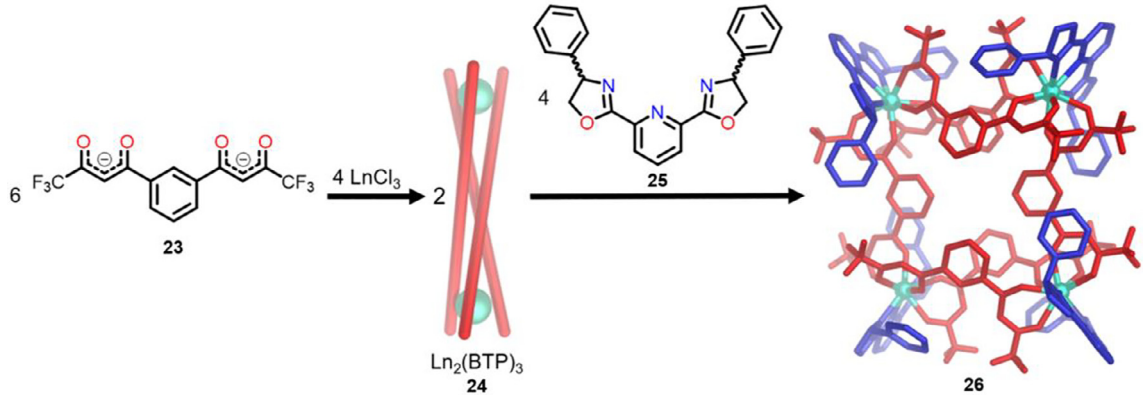

Scheme 2. Two-step self-assembly process of (**25**)$_4$Ln$_4$(**23**)$_6$ architecture (**26**) using BTP ligands (23) and Ph-Pybox co-ligands (**25**), through a bimetallic Ln$_2$(**23**)$_3$ helicate (**24**). (BTP = red, Ph-Pybox = blue) [42].

being a single BTP ligand within the lanthanide plane. Several π-π interactions between a phenyl group on Ph-Pybox molecules and the single BTP ligand were hypothesized to stabilize the heteroleptic architecture, promoting the circular helicate over a bimetallic triple-stranded helicate.

3.1.2. Tetrahedra

Two types of tetrahedra have been defined: i) face-capped Ln$_4$L$_4$ tetrahedra, typically comprised of tritopic C_3-symmetric ligands, and ii) edge-bridged Ln$_4$L$_6$ tetrahedra comprised of ditopic linear ligands (Fig. 8). Unlike simpler helicates, tetrahedra frequently exhibit internal void space allowing for encapsulation of small molecules and ions. Judicious choice of the coordinating moiety may enable formation of a complex where the luminescent properties arising from the Ln(III) metal vertexes are preserved. However, there are currently no examples of water-stable lanthanide tetrahedra reported; this limited aqueous stability restricts their application within biological contexts.

3.1.2.1. Face-capped Tetrahedra. More examples of face-capped tetrahedra constructed with lanthanide ions have been reported than for their edge-bridged counterparts. This is in part due to the observation that self-assembly of C_3-symmetric ligands in a 1:1 stoichiometry with lanthanide ions forms tetrahedral complexes with Ln$_4$L$_4$ formula in the vast majority of cases. By contrast,

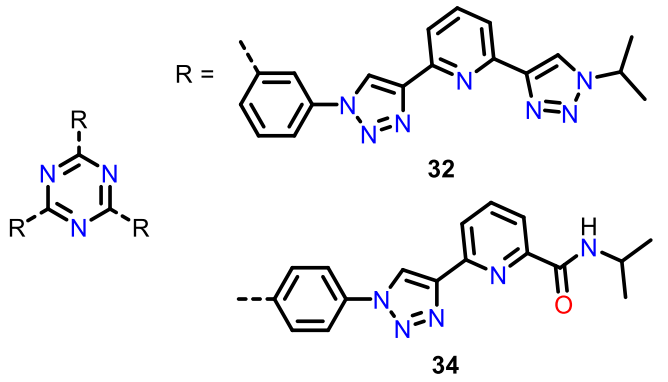

Fig. 12. Two C_3-symmetric ligands, **32** and **34**, synthesized by Sun and coworkers, featuring a triazine core and triazole-containing binding sites [72,73].

ditopic ligands can form other architectures [38,40,59,63], most notably triple-stranded helicates (see Section 3.1.1) and the occurrence of these non-tetrahedral architectures is far more prevalent than for tritopic ligands. In 2008, the single crystal X-ray structure of a $[Tb_4L_4]^{12+}$ face-capped tetrahedral complex (**27**; Fig. 9) was reported alongside solution state data that indicated isostructural Eu(III), Lu(III) and Tb(III) complexes of this form were stable in acetonitrile [64]. Isolation of **27** followed precedent for similar structures generated with transition metal vertices and thermodynamic analysis indicated that intramolecular binding of the tripodal receptor was disfavored [65]. As predicted, each metal ion was nine coordinate with three ligands coordinated through three atoms each. A subsequent publication by the same authors expanded the range of metals employed in the $[Ln_4L_4]^{12+}$ tetrahedron synthesis to include La(III)-Lu(III) and Y(III) [66]. The authors found that the thermodynamic stability of tetrahedral complexes comprised of lanthanides with ionic radius r > 1.13 Å was significantly decreased compared with metals with smaller ionic radii.

For the tetrahedra constructed from the amide bridged ligand (**28**), no appreciable void volume was observed as the methyl group on the central carbon of the C_3-symmetric ligand was directed into the center of the capsule. Variation of the ligand to generate an ester linkage (**29**) allowed access to structurally related $[Ln_4L_4]^{12+}$ structures which could accommodate guest anions within their central void pockets [67], however the limited size of these cavities restricted the range of guests which could be accommodated (Fig. 10).

Larger C_3-symmetric ligands were thus targeted including **30** (Fig. 11) which incorporated a rigid triptycene unit at its core [68]. Self-assembly of **30** with europium perchlorate yielded the desired $[Eu_4L_4]^{12+}$ complex (**31**) displaying ligand sensitized luminescence of the europium(III) center. The capsule was also shown to selectively bind guests paving the route for development of lanthanide-based cages for separation and sensing applications (see Section 4). Further work looked to modify the substituents on the triptycene centered ligands to improve the solubility of both the parent ligand and its metal complexes within water. Polyethyleneglycol (PEG) chains were appended onto the 4-position on the pyridyl moiety within the lanthanide ion binding sites and did indeed improve the complexes solubility in water [69,70].

More recently, Sun and coworkers have reported a series of complexes based on C_3-symmetric ligands built around a triazine core. Ligand **32** (Fig. 12), incorporating a triazole-pyridine-triazole chelating group generates complexes with a range of trivalent lanthanides (Pr, Nd, Sm, Eu, Tb, Dy, Ho, Er, Tm, Yb) which emit light in the visible and near-infrared regions [71]. The 82 % quantum yield reported for the $[Tb_4(\mathbf{32})_4]^{12+}$ tetrahedron (**33**) is particularly noteworthy and highlights the potential for these materials as photoluminescent devices. The outstanding luminescence properties of these complexes are in contrast to properties observed with similar ligands incorporating amido-pyridine-triazole chelators. Time dependent density functional theory (TD-DFT) studies indicate that the amido groups alter the direction of the electron transfer directly from the central triazine core, which may affect the lanthanide sensitisation. The connectivity of the triazole-pyridine-triazole chelating groups has also been shown to dramatically affect the self-assembled product. The ligand **34**, can also form $[Ln_4L_4]^{12+}$ tetrahedra but more frequently generated $[Ln_3L_3]^{9+}$ sandwich structures which displayed interesting luminescence properties due to the π-π stacking but have no internal void space [72].

Pyrene and pyrene-based guests proved effective in facilitating a transformation between $Ln_3(\mathbf{34})_3$ sandwich-like molecules and $Eu_4(\mathbf{34})_4$ tetrahedra, but smaller polyaromatic hydrocarbons, such as naphthalene, were less effective [73]. The chirality of the $Eu_4(\mathbf{34})_4$ tetrahedra formed were also affected by guest molecules. Achiral guests, such as pyrene, produced racemic mixtures of ΔΔΔΔ and ΛΛΛΛ Eu_4L_4 tetrahedra, whereas chiral molecules, such as *R*/*S* BINOL, resulted in enantiopure tetrahedra [73].

Yan and coworkers have also expanded the chiral auxiliary strategy they employed with helicates (Section 3.1.1) to the diastereoselective synthesis of face-capped cages. Utilizing tritopic β-diketonate ligands, **35**, and chiral S-BINAPO (**36**) selective formation of the ΛΛΛΛ-Eu_4L_4 cage **37** was achieved (Fig. 13) [74]. Moreover, when the chiral auxiliary, S-BINAPO, was replaced by an achiral auxiliary ligand, DPEPO, under the correct conditions,

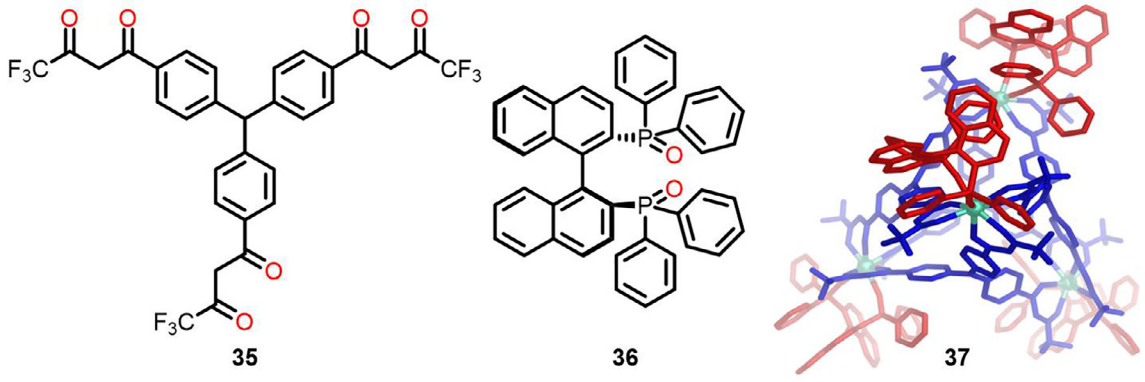

Fig. 13. Structures of **35** (right, blue), S-BINAPO co-ligand **36** (middle, red) and the crystal structure of $Eu_4(\mathbf{35})_4(\mathbf{36})_8$ architecture **37** [74]. (For interpretation of the references to colour in this figure legend, the reader is referred to the web version of this article.)

the chirality imprinted by *S*-BINAPO was retained. The ability to replace the chiral auxiliary with a less costly achiral alternative presents a promising route to the generation of enantiomerically pure cages and highlights another opportunity for lanthanide cages over their transition metal counterparts. In contrast to trivalent lanthanides, the low coordination numbers of transition metals make them less amenable to incorporation of exchangeable chiral components.

In addition to the high symmetry complexes discussed thus far, face-capped tetrahedral cages derived from lower symmetry tridentate ligands have also been reported [75]. 'Warped' Ce_4L_4 tetrahedra retained pseudo-C_3 symmetry and encapsulated appreciable void volumes that size-selectively accommodate guest molecules. Size-selective cyanosilylation reactions were demonstrated with these capsules when appropriately sized guests were employed. In the absence of the capsule, the corresponding reactions did not take place.

3.1.2.2. Edge-bridged Tetrahedra. As with face capped tetrahedra, much work has been done to explore the parameters governing the self-assembly of edge-bridged tetrahedra and optimization of their host and luminescent properties. Several systems have been reported that allow exclusive formation of edge bridged Ln_4L_6 tetrahedra [76], however it is more common that they are found in equilibria with Ln_2L_3 helicates [63,76,77]. Where mixtures are observed, the distribution of products is shown to be concentration-dependent, with higher concentrations favoring the larger tetrahedral complexes according to Le Chatelier's principle. A comprehensive explanation for the helicate to edge-bridged cage transition has previously been reported by Piguet [78].

Iterating on previous research by Raymond and coworkers [3], who reported offsetting transition metal binding sites in bitopic ligands increased the favorability of larger architectures being formed, Sun and coworkers studied a series of linkers of similar length with varying degrees of binding site offset (Fig. 14) [63]. Their results followed the previously reported trend: complexations with **38** resulted in Ln_2L_3 architectures exclusively whilst an increase in offset, using a stilbene linker, **39**, resulted in a mixture of helicate and tetrahedron. Additional offsetting by a naphthyl linker, **40**, yielded tetrahedral architectures exclusively.

Further research into the effects of linkers on architecture formation was investigated by Law and coworkers, *via* the employment of 1,4-phenyl-based linkers [77]. These linkers did not induce offsetting between binding sites, instead increasing the distance between binding sites. For all ligands (**41**–**43**) (Fig. 15), Eu_2L_3 helicates were isolated, whilst edge-bridged tetrahedra formed from ligand **41** only. In solution, $Eu_4(\mathbf{41})_6$ slowly reverted to the equivalent complex $Eu_2(\mathbf{41})_3$. The rate of conversion from Ln_4L_6 to Ln_2L_3 within this system was studied with a range of lanthanide ions, to determine how ionic radius would affect tetrahedral stability. Larger ions favored the smaller architecture, with no evidence for the conversion to the $La_4(\mathbf{41})_6$ tetrahedra. Conversely, smaller ions resulted in the formation of more stable tetrahedra, with $Lu_4(\mathbf{41})_6$ exhibiting negligible conversion to $Lu_2(\mathbf{41})_3$ helicate after 10 days.

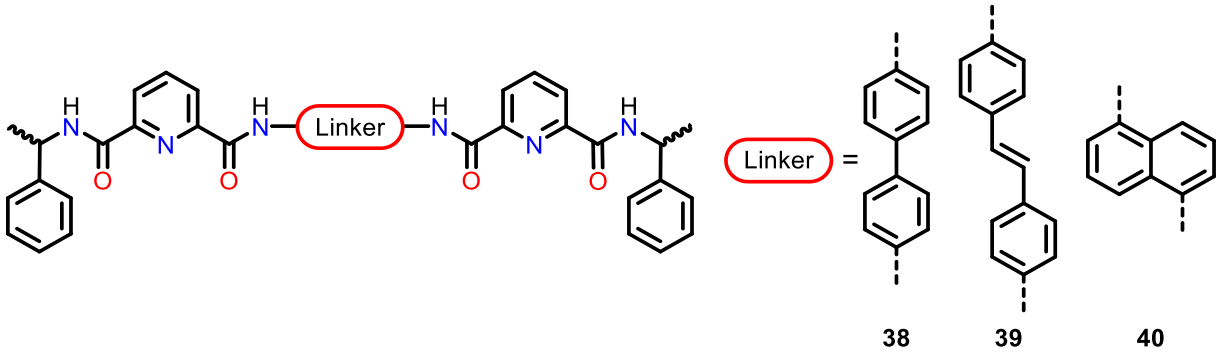

Fig. 14. Three ligands (**38**, **39** and **40**) used by Sun and coworkers to investigate the effects of increasing binding site offsetting on architecture speciation following complexation reactions with lanthanide salts [63].

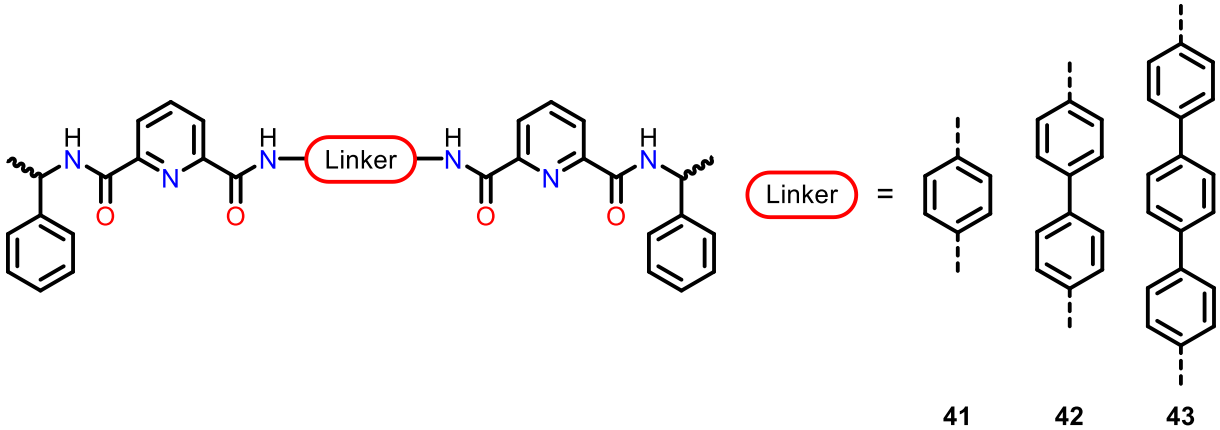

Fig. 15. Three ligands (**41**–**43**) synthesized by Law and coworkers to study linker length influence on the architecture formed *via* complexation reactions with lanthanide salts [77].

The stereoselective formation of edge bridged cages has been explored by Sun and Law [43,79], both of whom employed chiral ligands to direct the metal chirality. An initial publication by Sun and coworkers detailed the first stereocontrolled synthesis and characterization of lanthanide tetrahedra. Both edge bridging and face capping ligands with *R*- and *S*- stereochemistry were reported in this publication and ligand sorting phenomena were also discussed. Solution CD spectra confirmed the enantiopurity of the Eu_4L_6 and Eu_4L_4 structures with CD spectra for pairs of enantiomeric cages appearing as mirror images of each other. Furthermore, the introduction of the chiral TRISPHAT anion ([tris (tetrachlorocatecholato)phosphate]$^-$) to the enantiomeric cages generated diastereomeric pairs, which were distinguishable using ^{1}H NMR spectroscopy [80]. Having established the enantiomeric purity of the cages, the authors then explored the sorting behavior of the ligands. Not unsurprisingly when two- and threefold symmetric ligands were combined within one reaction mixture alongside europium perchlorate, narcissistic sorting dominated resulting in two populations of cages: edge bridge and face capped, respectively. However, when two bis(tridentate) ligands, L^R and L^S were mixed with europium perchlorate, a statistical mixture of Eu_4L_6 cages was formed with varying numbers of *R*- and *S*- stereochemical ligands. In contrast to this, under the same conditions mixtures of *R*- and *S*- tris(tridentate) ligands with europium perchlorate generated a racemic mixture of the two homochiral cages (ΔΔΔΔ and ΛΛΛΛ.) The authors propose this differential behavior between the edge bridged and face capped tetrahedra likely arises due to stronger mechanical coupling in the Eu_4L_4 cages versus the edge bridged Eu_4L_6 counterparts.

Building on this initial publication, in 2017 Law and coworkers published a systematic study that linked the positioning and bulk of a chiral substituent on a ligand with the chiroptical response taking the field of luminescent chiral cages one step closer to the rational design of materials with potential applications. This paper provided the first circularly polarized luminescence (CPL) spectra for lanthanide cages; this technique provides a more direct read out of chiral information at the emitting Eu center than CD spectroscopy. The CPL signal strength correlated with the overall screw sense of the cages, which is dictated by the chiral ligands, with **44** > **46** > **45** (Fig. 16). Chiral amplification experiments revealed a non-linear CD response as the percentage of chiral **39** changed indicating cooperative stereochemical coupling between metal centers. These results indicate that not only the inclusion but also the positioning and bulk of a chiral substituent on organic ligands should be considered when designing enantiopure lanthanide cages.

3.1.3. Larger multinuclear architectures

While initial self-assembly studies typically generated helicates and tetrahedra, several larger and more complex lanthanide architectures have been reported as the field has matured including cubes, trigonal prisms, octahedra and tetrapods. Many of these structures have a greater internal void volume to ligand length ratio and larger pores, allowing for encapsulation of larger species.

In 2017 Sun and coworkers reported the first example of a supramolecular cube [63]. The edge-bridged Ln_8L_{12} species was synthesized from a bistridentate ligand containing a central anthracene panel at ligand concentrations of 40 mgmL^{-1} or upon crystallization. At lower ligand concentrations the simpler Ln_2L_3 helicate was observed to form. The crystal structure of a Nd_8L_{12} cube revealed extensive π-stacking; six sets of five component ADADA (acceptor–donor-acceptor–donor-acceptor) stacks provide a strong driving force for the assembly of this large complex. A complementary face-capped Ln_8L_6 cubic species has also been reported that incorporates tetratopic C_4-symmetric porphyrin-based ligands (**47**; Fig. 17) [81]. The cubic structure could be directly self-assembled with Eu(III), Pr(III) or Nd(III) as the metal ions, but could be accessed through post-synthetic metal exchange, or *via* structural transformation of a Ln_6L_3 trigonal prism complex when $Yb(OTf)_3$ was employed as the metal salt. The authors propose competing coordination binding and ligand torsion events direct the outcome of the final product, as well as the kinetics of error correction which have previously been shown to significantly differ for lighter and heavier lanthanides [82]. Single crystal X-ray diffraction analysis of the Yb_8(**47**)$_6$ cube indicated a large internal void space (1291 Å^3), coupled with the aromaticity of the central porphyrin moiety this allowed for encapsulation of aromatic molecules (perylene, 1,12-benzoperylene and coronene.).

A series of lanthanide polyhedra with general formula $M_{2n}L_{3n}$ have also been reported [83]. The structures ranging from Ln_4L_6 to $Ln_{10}L_{15}$ stoichiometries employ a novel 2,6-pyridine bitetrazolate binding moiety (Fig. 18) in a family of non-linear bitopic ligands, and are, to date, the only examples of water soluble lanthanide architectures with internal void space. In particular, the Eu_8L_{12} complex (**48**) has good water solubility and luminescence quantum yield, whilst the Eu_8L_{12} analogue and longitudinal relaxivity properties making it a promising structure for use in bioimaging (see Section 4.4).

Employing tripodal ligands, with two binding sites per arm (**50**; Fig. 19) Hamacek and coworkers generated an unusual Eu_8L_6 tetrapodal architecture (Fig. 19) [84]. A molecular model of the octanuclear complex was validated using small angle X-ray scattering (SAXS) data since only poor diffraction data could be obtained for this complex. As with most supramolecular architectures, a racemic mixture of homochiral tetrapodal architectures was found to exist in solution.

The crystal structure and magnetic properties of an octahedral ($Ln_{12}L_{12}$) architecture incorporating twelve dysprosium(III) ions has also been reported. The ditopic ligand incorporates two

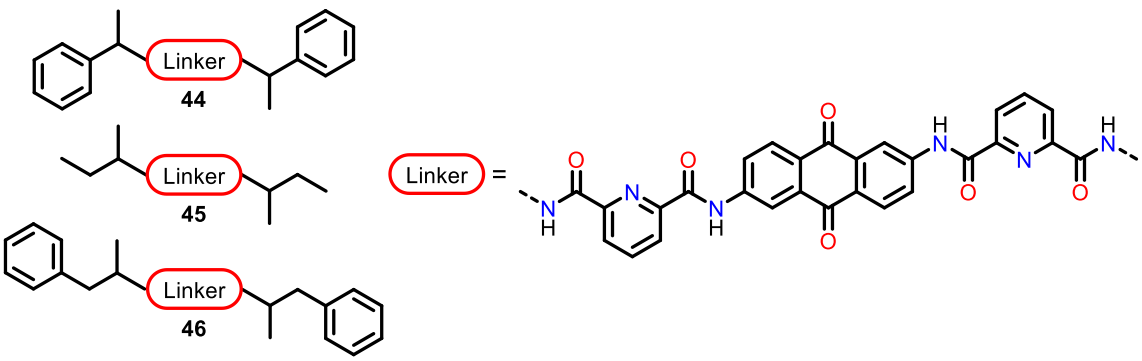

Fig. 16. Three ligands (**44**–**46**) synthesized by Law and coworkers, to investigate how functionalisation of terminal amide groups affect the chiral luminescence properties of lanthanide architectures [79].

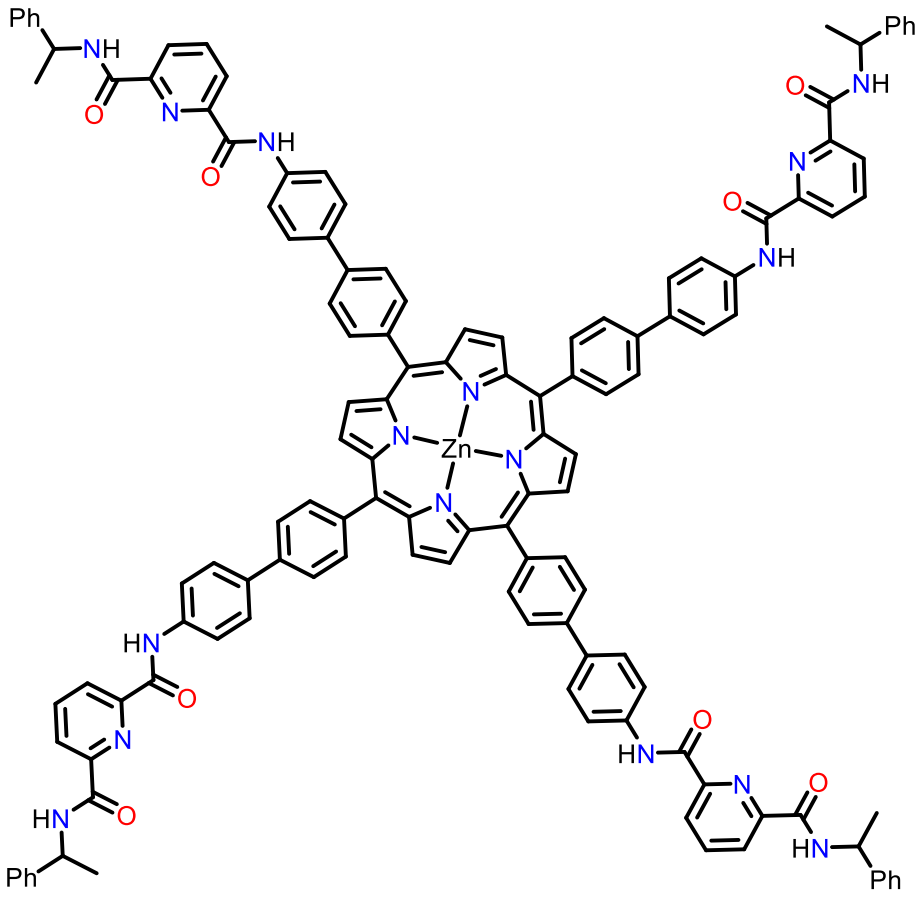

Fig. 17. Metalloligand, **47**, synthesized by Sun and coworkers, used in the formation of a Ln_8L_6 face-capped cube [81].

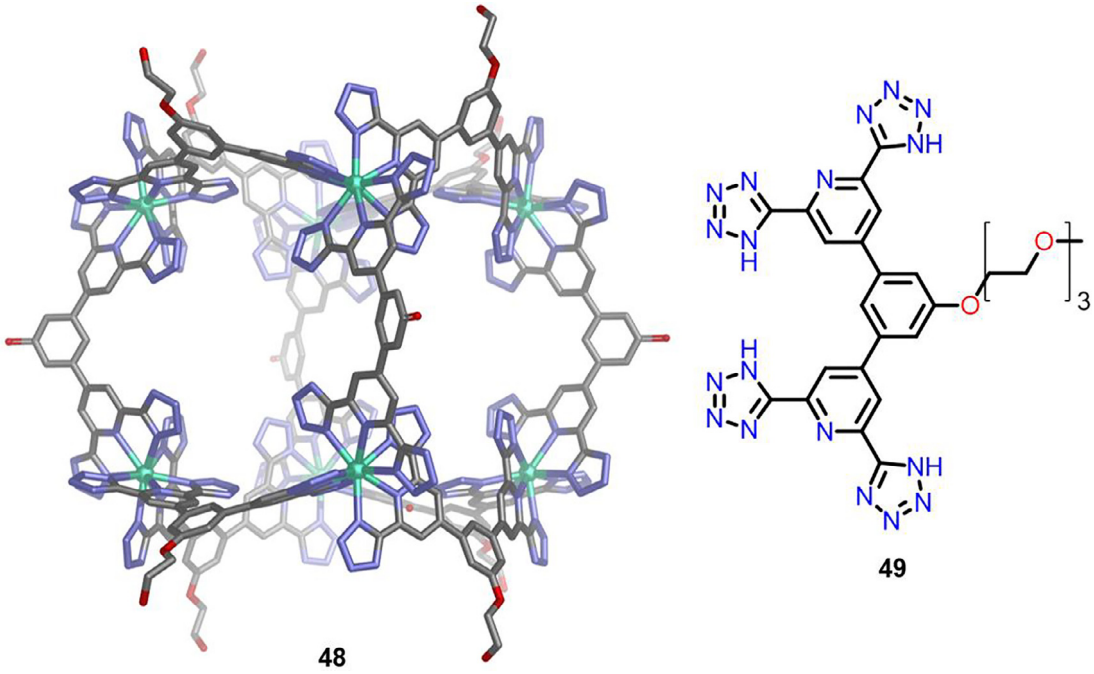

Fig. 18. Single crystal X-ray structure of a 'waterproof' Eu_8L_{12} architecture (**48**) synthesized by Sun and coworkers (left) and the ligand **49** (right) from which it is constructed. PEG chains have been omitted or simplified in the crystal structure schematic [83].

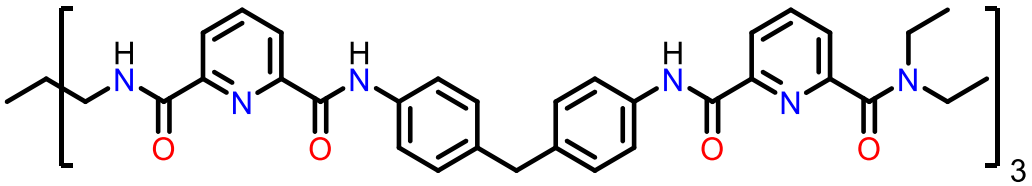

50

Fig. 19. Hexatopic ligand, **50**, synthesized by Hamacek and coworkers [84].

tetradentate binding pockets, which necessitates each vertex of the octahedron to accommodate two lanthanide ions to satisfy the ligand coordination sites. Additional metal coordination sites are occupied by solvent and counterion molecules. This pairwise incorporation of metal ions is unusual in supramolecular coordination chemistry but clearly provides a route to access structures not accessible through the more traditional single metal ion per vertex design approach.

Recently, sterically hindered organic linkers were shown to be useful for the formation of lanthanide based architectures with missing bridging ligands [85]; this methodology provides an alternative route to less traditional multinuclear structure types. Three ligands with structural variations, designed to investigate the effect of inclusion of bulky substituents in different positions on the ligands, were synthesized, **51**–**53** (Fig. 20). When combined with a range of trivalent lanthanide salts of Eu, Sm, Gd, and La, **51** generated a M_8L_{10} cube-like structure with two missing ligands. Analysis of the crystal structure revealed the Eu-Eu metal distances were shortened by over 7 Å along the edges which were not bridged by a ligand. Ligand **52,** which had increased backbone rigidity in comparison to **51,** generated a M_4L_5 tetrahedron-like architecture with one edge missing, while the longer ligand (**53**) allowed some of the internal strain of the system to be relieved to generate a fully saturated M_6L_9 trigonal prismatic structure. Coordination at metal sites which were not saturated by ligand was fulfilled by water molecules. Formation of supramolecular architectures which incorporated defects, generated structures that were able to accommodate a number of bulky guests due to increased portal sizes and adaptability of these capsules. Additionally, the generation of complexes with open metal sites also presents exciting possibilities for sensing, separation and catalytic applications.

3.2. Heterometallic structures

A limited number of supramolecular architectures containing both transition metal and lanthanide ions exist. Advantages of these systems over metal–organic structures self-assembled from only lanthanide ions include the opportunity to pair the strong absorption from transition metal ions with the luminescent properties of lanthanides ions. Additionally, the relatively robust and well-defined coordination properties of transition metals may allow for the formation of architectures incorporating both d and f metals which are less kinetically labile then those generated in the absence of transition metals.

An array of transition metal-lanthanide bimetallic triple-stranded helicates have been reported utilizing ditopic pentadentate ligands (Fig. 21) [86–96]. First row transition metal ions are the most commonly reported, although second [86,87] and third row transition metal ions [88] have also been employed. The first example, a Zn**Ln54**$_3$ helicate, was synthesized by Bünzli and coworkers in 1995. A 1:1:3 Zn: Ln: **54** stoichiometry was employed to promote the desired structure however the homonuclear helicates (Zn_2**54**$_2$ and Ln_2**54**$_3$) were also observed to form [89]. All Ln(III) ions were capable of forming the Zn**Ln54**$_3$ species [90], however it was observed that when the Zn(II) ion was substituted in place of the Fe(II) ion only the larger lanthanide ions (La-Eu) yield the desired Fe**Ln54**$_3$ complex [91,92]. Replacement of zinc within these structures also enabled investigations into the magnetic properties of these heterometallic helicates. The spin crossover behavior of Fe**Ln54**$_3$ complexes were evaluated, with all species exhibiting incomplete gradual spin crossover between 240 and 340 K. Minor differences in the proportion of high-spin Fe(II) centers were observed with different lanthanide ions, these differences were hypothesized

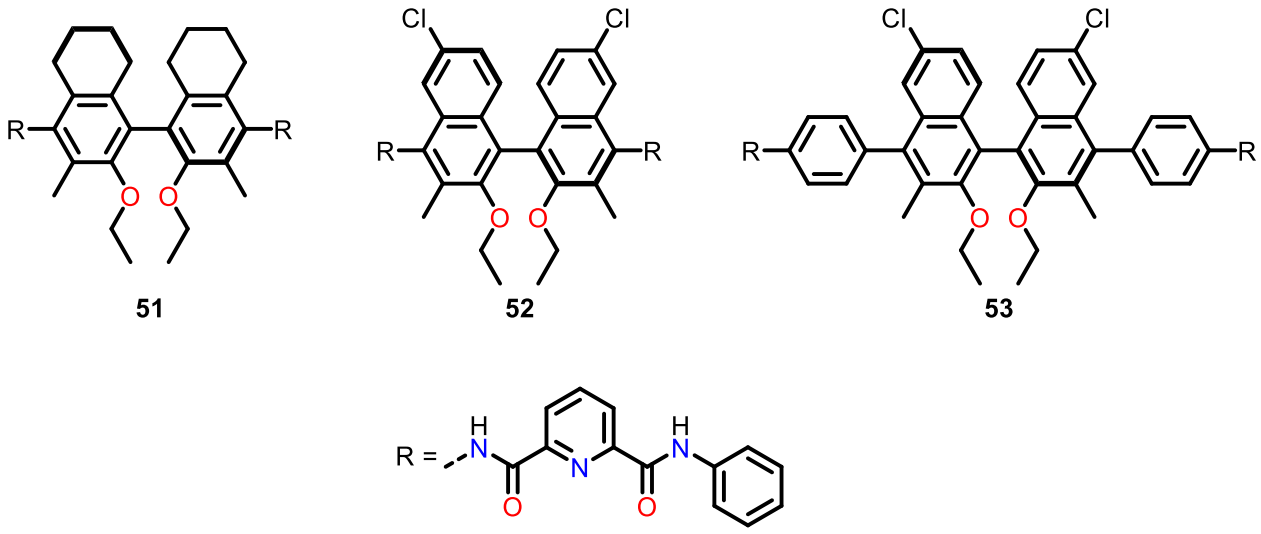

51 **52** **53**

Fig. 20. Three ligands (**51**–**53**), with bulky BINOL-based linkers, synthesized by Liu and coworkers, which yielded novel lanthanide architectures including an M_8L_{10} cube like structure, an M_4L_5 tetrahedron missing one edge and an M_6L_9 trigonal prism, respectively [85].

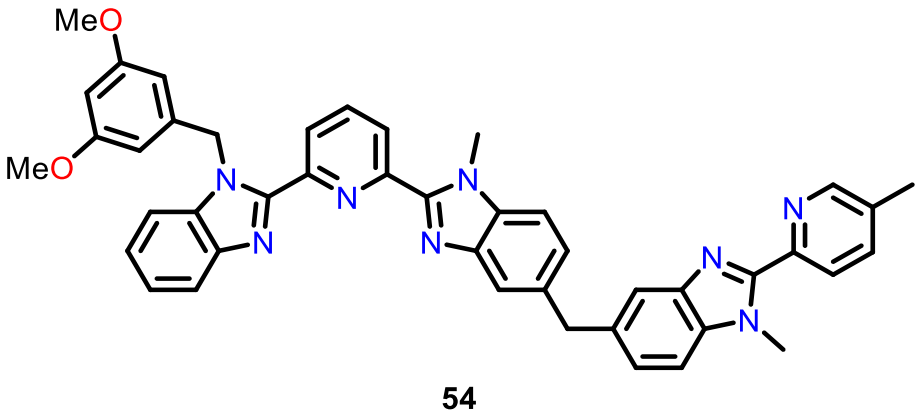

54

Fig. 21. Ligand **54**, synthesized by Bünzli and coworkers [89].

to be influenced by variations in the Fe(II) coordination geometry.

The luminescent properties of a heterometallic Fe-Ln complex were also investigated, with major differences observed between high-spin and low-spin Fe(II) ions due to the marked difference in absorption between the spin states [93]. The introduction of a Cr(III) ion rather than Fe(II) or Zn(II) ions, resulted in large changes in the luminescence behavior of the complex [93]. Lanthanide(III) → Cr(III) energy transfer processes were observed for Tb(III) and Eu(III) and resulted in enhanced Cr(III)-centered luminescence, dependent on the energy overlap between the excited lanthanide and Cr(III) energy levels. Improvements in water solubility were sought *via* the incorporation of terminal carboxaldehyde [95] or carboxylate moieties [96], in place of the terminal benzimidazole moiety **54**. The improvement in water stability was accompanied by significant luminescence increase attributed to less frequent luminescence depleting interactions with solvent molecules.

The incorporation of a single terminal bidentate and two tridentate binding moieties within a linear ligand (Fig. 22) resulted in the formation of a HHH $ZnLu_2$**55**$_3$ helicate in a 1:2:3 Zn: Lu: **55** stoichiometry [97]. The Zn(II) occupies the tris(pyridine-benzimidazole) cavity in an octahedral geometry, whereas both Lu(III) ions have a coordination number of nine. However, a wide array of species were observed when the stoichiometry of the starting materials was altered. A structurally related trimetallic helicate featuring two terminal transition metal and a central lanthanide binding site (Fig. 23) was also reported by Piguet and coworkers [98].

Three triple-stranded Fe(III)-Gd(III) structures were reported by Raymond and coworkers (Fig. 24) utilizing bidentate 1-hydroxypyridin-2-one and terephthalamide (HOPO and TAM, respectively) binding sites displaying preferential metal ion binding [99]. Bi and tri-metallic helicates were obtained utilizing ligands **58** and **59**, whilst a third architecture was formed through an iron-facilitated imine condensation with TREN, which generated ligand **57**. The bidentate Gd(III) binding site allows for water molecules to bind to the metal center, which allows for this class of architecture to be investigated as MRI contrast agents.

An elegant early example of a supramolecular complex incorporating d and f metals was reported by Yanagida and coworkers [100]. The two-dimensional square (**60**) incorporated two octahedral Ru(II) ions alongside two Ln(III) ions (Fig. 25) and was formed by addition of [Ru(2,2′-bpy)$_2$(4,4′-bpy)$_2$] to a Ln(TTA)$_3$ complex in solution where Ln = Nd or Yb and TTA is = 2-thenoyltrifluoroaceto nate. Two 2,2′-bipyridyl (bpy) ligands were observed to bind facially to the Ru(II) center in solution resulting in two 4,4′-bpy ligands extending 90° from each other as monodentate ligands. In the final structure, the unsaturated binding sites from the starting Ln(TTA)$_3$ complex are complexed by the 4,4′-bpy ligands to generate a square architecture of the form [(2,2′-bpy)$_2$Ru]$_2$(4,4′-bpy)$_4$[Ln(TTA)$_3$]$_2$ (**60**). This architecture exhibits luminescence sensitization through the strong metal to ligand charge transfer (MLCT) absorption of the transition metal complex, allowing near-infra-red emission from Nd(III) ions; this may pave the way for in vivo studies of lanthanide architectures due to increased penetration capabilities of longer wavelengths through organic matter, such as skin.

In 2015 Tang and coworkers reported the synthesis of a molecular square incorporating transition metal ions at the midpoint of the edge, and dysprosium ions at the vertices (Fig. 26) [101]. Initially the transition metal site was occupied by Cu(II) ions, but further research expanded the scope to include Co(II) and Zn(II) ions at this site generating multinuclear TM(II)-SCN clusters [102]. A single water molecule was also observed bound to the metal center to satisfy the Dy(III) coordination sphere.

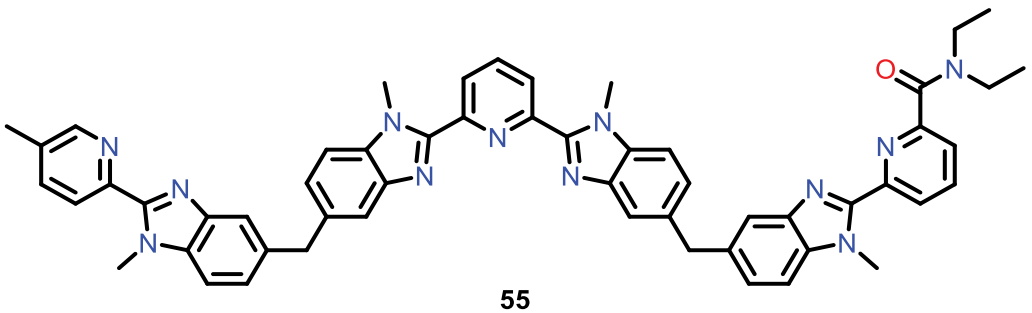

55

Fig. 22. Ligand **55**, synthesized by Piguet and coworkers designed to binding to octahedral transition metal and lanthanide ions [97].

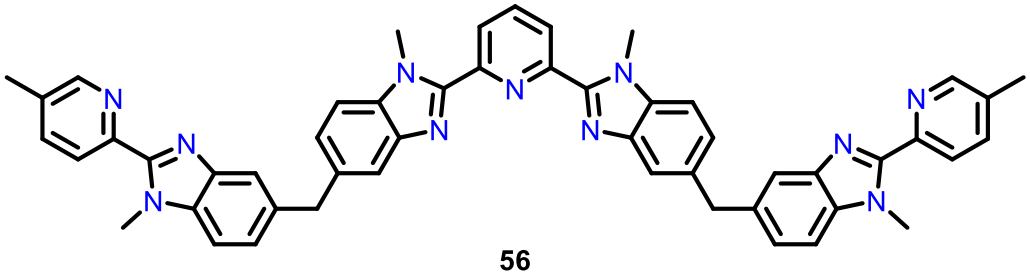

56

Fig. 23. Ligand **56**, synthesized by Piguet and coworkers, that yielded a $Zn_2Ln\mathbf{56}_3$.

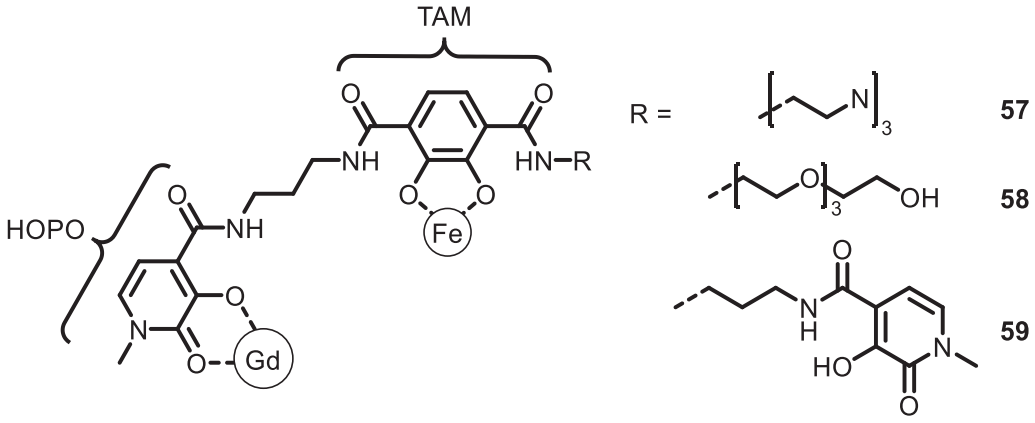

Fig. 24. Three ligands (**57**–**59**) synthesized by Raymond and coworkers, showing the binding sites of the Fe(III) and Gd(III) ions [99].

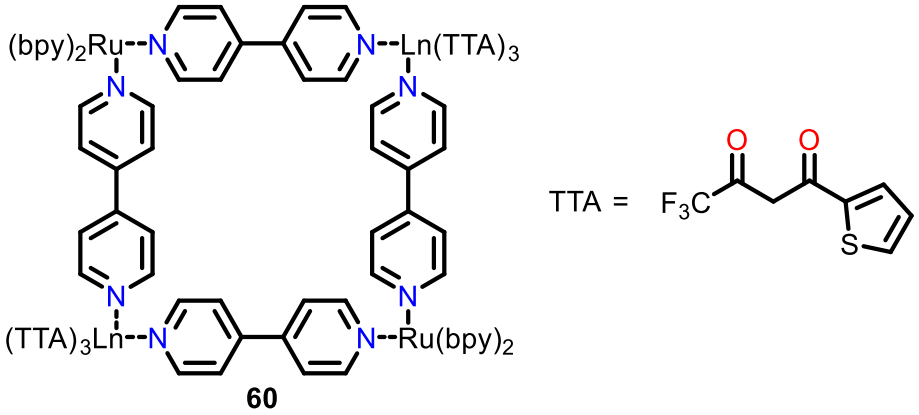

Fig. 25. Structure of 2D heterometallic Ru_2Ln_2 square architecture **50** synthesized by Yanagida and coworkers (left), and structure of TTA (right) [100].

A transition metal-lanthanide trigonal bipyramidal architecture [103] has also been reported following a similar step-wise synthetic protocol. A heteroditopic ligand featuring a dipicolinamide binding site, and a terminal imidazole moiety was introduced into a solution containing *cis*-blocked dipalladium 2,2′-bipyridyl clips. This solution yielded a (2,2′-bpy)Pd_2L_2 species with the imidazole moiety bridging between two palladium centers. This resulted in a 90° angle between the dipicolinamide binding sites. Three dipalladium complexes, each with two terminal dipicolinamide binding sites were employed to saturate two lanthanide coordination spheres. The final architecture was defined as a $Ln_2((2,2'\text{-bpy})_2Pd_2L_2)_3$ trigonal bipyramid. Following assembly and characterization, luminescence titrations were conducted on the complex with a series of antibiotics. Rapid luminescence quenching was observed upon addition of β-lactam based antibiotics. Further analysis of the solution indicated (2,2′-bpy)Pd_2L_2 was liberated upon addition of the antibiotics suggesting these molecules underwent competitive binding to the lanthanide ions, with no disruption of the Pd-L bond.

Research has also moved towards synthesizing architectures with multiple different lanthanide ions present within one complex. As helicates are the simplest architecture, they are at the forefront of the field. Numerous binding sites were probed within mononuclear LnL_3 complexes, with the complex stability in acetonitrile being evaluated. Picolinic acid based binding sites, were shown to favor metals with smaller ionic radii, with LuL_3 complexes being shown to be orders of magnitude more stable than the lanthanum equivalent. On the other hand, the benzimidazole binding site favored larger lanthanide ions; lutetium(III) was found to be 8000 times less stable than the gadolinium(III) analogue. When these binding sites were incorporated into ligands capable of generating helicates, the observed trends in stability were pre-

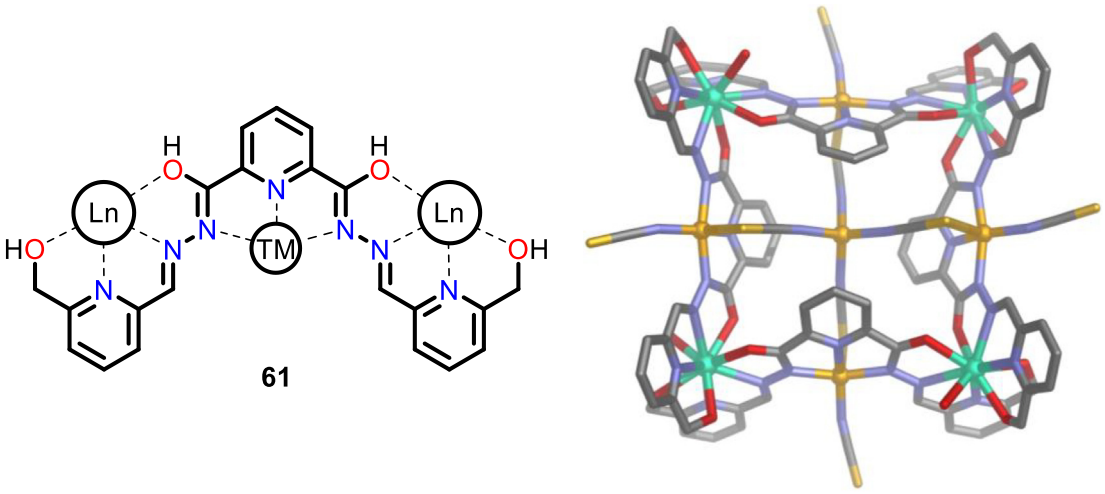

Fig. 26. Ligand **61**, indicating location of transition metal and lanthanide binding sites (left), and the structure of $Dy_4Cu_5\mathbf{61}_4(SCN)_8.(H_2O)_4$ (right) [102].

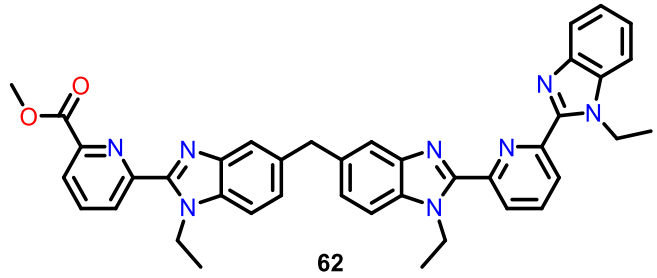

Fig. 27. Structure of heteroditopic ligand (**62**) synthesized by André and coworkers, used in the formation of hetero-lanthanide helicates [50].

served, and indeed amplified by 2–3 orders of magnitude [50]. This led to the development of heterotopic ligands, allowing selective binding of two different lanthanide ions. When stoichiometric amounts of La(III), Lu(III) and the heterotopic ligand (**62**; Fig. 27) (1:1:3) were heated in acetonitrile, hetero-lanthanide helicates formed with up to 90 % of the ligands within the helicates having aligned in the same way. These structures were termed head:-head:head, or HHH helicates. As differences in the ionic radii between the lanthanide ions decreased, helicate selectivity also decreased, and a higher proportion of homometallic helicates, as well as head:head:tail (HHT) helicates were observed within the self-assembly reaction mixture.

In 2020, a heterobimetallic tetrahedron (**63**) featuring four zinc (II) ions on the vertices and four lanthanum(III) ions on the faces of the tetrahedron (Scheme 3) was reported [104]. The complex was formed *via* a sub-component self-assembly process with three ligand molecules (**64**) undergoing a ring forming imine condensation. The single crystal X-ray structure revealed La(III) ions coordinated to six nitrogen donor atoms of the macrocyclic face in

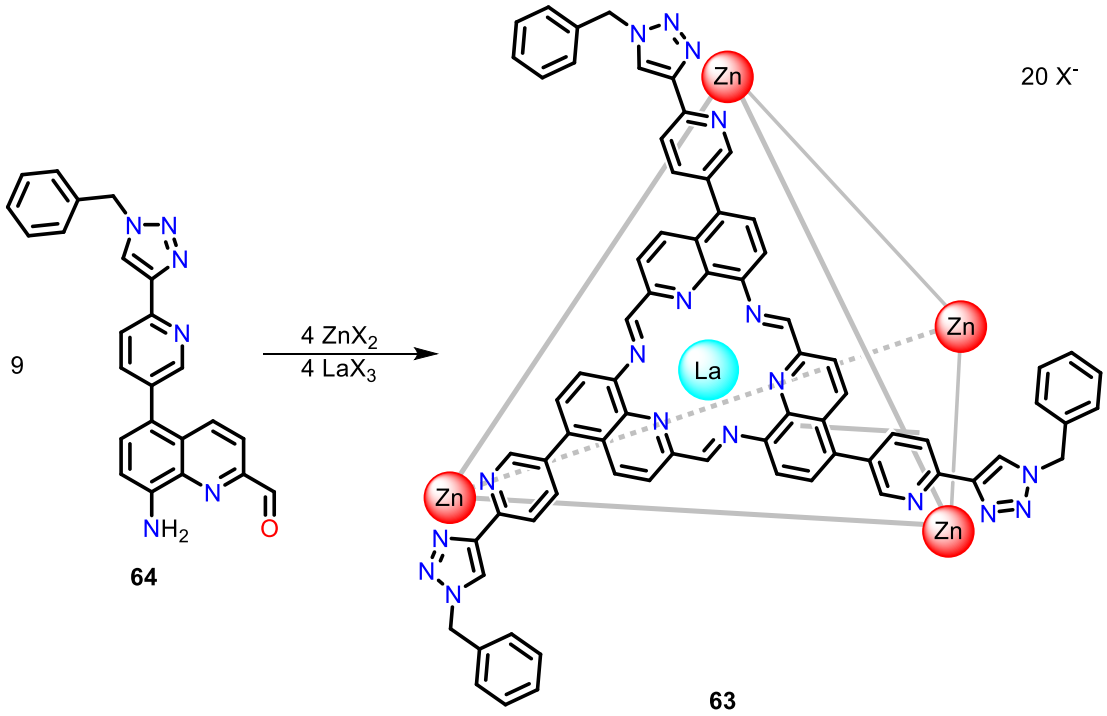

Scheme 3. Subcomponent self-assembly of $La_4Zn_4(64)_6$ (63) heterometallic tetrahedra *via* the addition of zinc(II) and lanthanum(III) salts to 64 by Nitschke and coworkers (X = OTf^- or ClO_4^-) [104].

addition to four water molecules. Three of these water molecules were directed out of the capsule while one per face was directed into the internal cavity of the complex. Despite the internally directed water molecules, the capsule still displayed good host–guest binding affinities for a range of small polyatomic anions (ClO_4^-, ReO_4^- and TfO^-), and these binding events were readily followed by luminescence spectroscopic titrations [104].

3.3. Peptide-based supramolecular architectures

An alternative approach to the formation of large multinuclear architectures featuring lanthanide ions has focused on peptides as ligands [105]. Various synthetic peptide α-helices, or coils, have been employed in this manner, with up to three peptides around central metal ions, termed 'coiled coils' or CCs [106–108]. Lanthanide ions are seldom observed in nature; however, their ionic radii and binding preferences are similar to Ca(II) allowing lanthanide ions to bind in calcium sites. Binding constants for Ca(II) versus Ln ions may vary significantly [109]. Early examples of lanthanide bound coiled coils utilized glutamic acid, although binding interactions were weak [110]. Binding interactions were improved by employing a functionalized, non-proteogenic glutamic acid, γ-carboxyglutamic acid. Aspartic acid (D) and asparagine (N) are commonly reported in more recent examples, where the amino acids are four positions apart [111]. Coiled coils with multiple bound lanthanide ions have yet to be reported, but a heterometallic ytterbium-mercury triple coiled coil species has been reported [107].

4. Applications

Supramolecular species such as the tetrahedral and cubic structures discussed above commonly have accessible internal void space [112]. This void space is frequently observed to accommodate small organic molecules [113] and/or counterions [67]. Encapsulation is driven by intermolecular interactions between the 'guest' and 'host' architecture. In the absence of these interactions, species of appropriate size to be encapsulated diffuse freely between the structure and bulk solvent spending negligible time encapsulated within the void space. Encapsulation is favored when the internal microenvironment of the capsule varies from that of the bulk solution and better matches the guest's preferred environment. Favorable encapsulation environments can modulate the reactivity of the guest molecule enabling functionality not observed under ambient conditions. This cavity-modified behavior has been exploited in catalysis (Section 4.1), sensing (Section 4.2) and separations (Section 4.3) as outlined below. On the other hand, the intrinsic properties of the trivalent lanthanide metal ions have been explored for applications in imaging (Section 4.4) and magnetism (Section 4.5).

4.1. Catalysis

Constriction within supramolecular assemblies is well established to lower a reaction's activation energy by providing alternative reaction pathways and may also alter the regioselectivity of the reaction products when compared with reactions performed in bulk solution [114].

Duan and coworkers synthesized three cerium(III) face-capped tetrahedra (Ce_4L_4) utilizing the novel C_3-symmetric ligands **65, 66** and **67** (Fig. 28), which each contained malonohydrazone binding sites [113]. These tetrahedra formed 1:1 host–guest complexes with a series of aromatic aldehydes as determined by spectroscopic studies. Spectroscopic titrations indicated that increasing aldehyde concentrations quenched the luminescence of the complex. Further studies probed the catalytic ability of the Ce_4L_4 complexes *via* the cyanosilylation of the encapsulated aldehyde. In the absence of the tetrahedra, cyanosilylation of the aromatic aldehydes did not occur with an acid catalyst added at room temperature over three days. Initial experiments with a catalytic load of 2 mol% of Ce_4L_4 resulted in yields ranging from 21 to 99 %. As expected, catalysis was size-dependent with the smallest tetrahedron Ce_4(**65**)$_4$, being an effective catalyst for benzyl aldehydes (86 – 99 % conversion) to the corresponding cyanohydrin silyl ether, although conversion rates dropped significantly for naphthyl aldehydes (20 – 68 % conversion). The larger Ce_4(**66**)$_4$ tetrahedra exhibited high conversion rates up to anthracene-based aldehydes, whereas the largest tetrahedra (Ce_4(**67**)$_4$) showed low conversion of all encapsulated aldehydes studied, as the internal void space was too large to direct the starting materials towards each other [113].

4.2. Sensing

In addition to catalysis, guest binding within lanthanide-based structures has been employed for sensitive and selective detection of small organic molecules and anions. Utilizing a water-soluble lanthanide helicate [21], Bünzli and coworkers evaluated the application of $[Eu_2L_3]^{6+}$ complexes as cancerous cell optical imaging agents. Cytotoxicity studies in HeLa cells indicated no change in cell viability up to 500 micro-molar concentration; this concentration is 50-fold higher than the concentration required to observe luminescence [23]. To date, no studies have been reported using multinuclear lanthanide architectures in vivo.

In 2017, Sun and coworkers reported luminescence quenching of a Eu_8(**35**)$_{12}$ cube upon encapsulation of nitro-aromatic molecules [63]. Quenching of the complex was attributed to two mechanisms. Firstly, the electron-deficient nitro-aromatic species forms a non-emissive ground state charge-transfer complex with an electron-rich ligand. The second pathway was a collisional mechanism, from the nitroaromatic to the lanthanide center, resulting in a decrease in luminescence lifetime. Encapsulation of picric acid rapidly quenched luminescence, with a 1.03 μM detection limit, suggesting that lanthanide architectures have potential application as a chemosensor for explosive materials.

A family of Ce_4L_4 tetrahedra incorporating amide groups within the ligand (Fig. 9, 68), have been developed with a view to forming cooperative hydrogen bonds with biologically important molecules including saccharides, ribonucleotides and tumor markers. Studies indicated that Ce_4L_4 tetrahedra synthesized with **66** and **68** displayed enhanced luminescence signals following encapsulation of saccharide molecules [37]. For the cage synthesized with **66** significant luminescence enhancement was observed for all monosaccharides tested, whilst only a small enhancement was observed upon encapsulation of disaccharides indicating a size-dependent interaction. The increased dimensions of **68** relative to **65** generated tetrahedral architectures with larger void space than the parent Ce_4(**65**)$_4$ cage. Simple models of **65** and **68** were used to calculate the volume of an ideal tetrahedral, with the internal void of the Ce_4(**68**)$_4$ tetrahedron being approximately-three times the size of the internal void of Ce_4(**65**)$_4$. Analysis of reactions containing mono- and disaccharides indicated that the disaccharide sucrose was selectively incorporated into the Ce_4(**65**)$_4$ cage with high selectivity over all other saccharides studied, including the disaccharides maltose and lactose. Selective sensing of sucrose over glucose and fructose, the monosaccharide constituents of sucrose, was also demonstrated. These results indicate that selective sensing for mono- and disaccharides is possible with cerium tetrahedra with complementary sized void cavities and hydrogen bonding patterns.

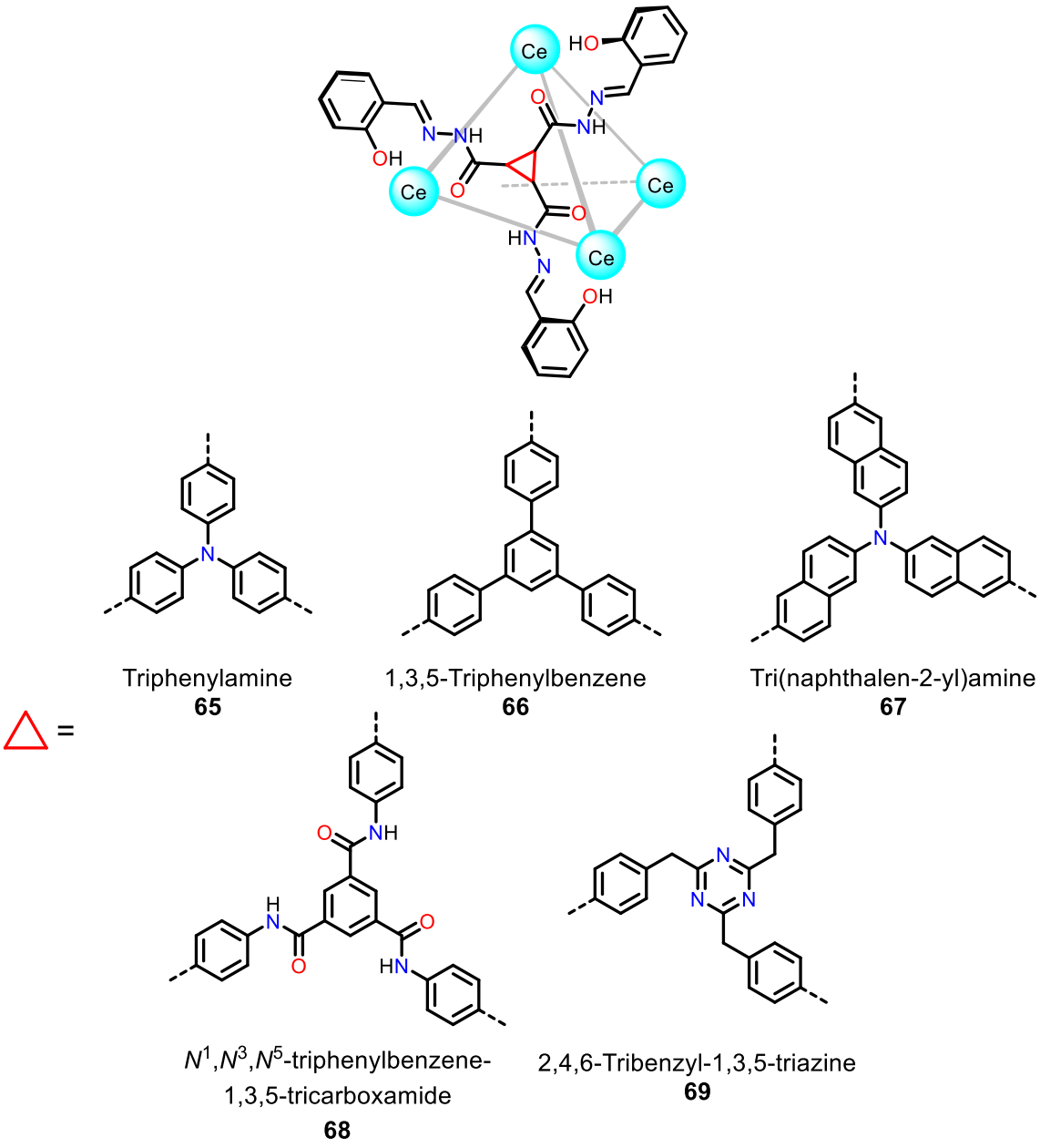

Fig. 28. Structure of three C_3-symmetric malonohydrazone-based ligands synthesized by Duan and coworkers. (Top left = triphenylamine linker (**65**), top middle = 1,3,5-triphenyl benzene linker (**66**), top right = tri(naphthalene-2-yl)amine linker (**67**), bottom left = N^1,N^3,N^5-triphenylbenzene-1,3,5-tricarboxamide linker (**68**), bottom right = 2,4,6-tribenzyl-1,3,5-triazine linker (**69**). Red triangle indicates tritopic linker [37,113,115,116]. (For interpretation of the references to colour in this figure legend, the reader is referred to the web version of this article.)

Using the structurally related triazine linker with malonohydrazone-based binding sites (**69**), Duan and coworkers reported the formation of a ribonucleotide binding Ce_4L_4 tetrahedron (Fig. 28). As with the previous examples, binding of the biomolecule resulted in a luminescence enhancement. Studies with nucleosides U(uracil), C(cytosine), A(adenine) and G(guanine) indicated a correlation between the number of hydrogen bonds the base could form with the cage and the luminescence intensity, with G demonstrating the strongest response [115]. In contrast to the luminescence enhancement observed with the nucleosides, the analogous ribonucleoside phosphates (mono-, di- and tri- G, U,C and A) showed muted luminescence enhancement with only guanosine monophosphate displaying a notable change in the luminescence signal. Selective detection of guanosine and guanosine monophosphate from the ribonucleotides investigated illustrates the potential application of lanthanide tetrahedra as highly selective chemosensors for biological molecules.

Duan and coworkers have also demonstrated the application of cerium cages generated with **65** as chemosensors for the tumor marker 5-hydroxyindoleacetic acid (5-HIAA) [116]. 5-HIAA is a common metabolite in urine, but is produced in much greater amounts by carcinoid tumors [117]. Encapsulation of 5-HIAA within the tetrahedra was observed by mass spectrometry, where one 5-HIAA was shown to be encapsulated per tetrahedra. Encapsulation of 5-HIAA was accompanied by a 2.5-fold increase in luminescence in a 9:1 dimethylformamide: water solution. Competition studies, using ten organic molecules commonly found in urine, indicated selective sensing towards 5-HIAA, as no significant change in luminescence was observed for any other species. Luminescence studies were performed in simulated urine, yielding

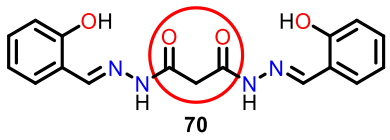

70

Fig. 29. Structure of hydrazine-based ligand (**70**) with methyl linker, highlighting central 1,3-β-diketone binding site [36].

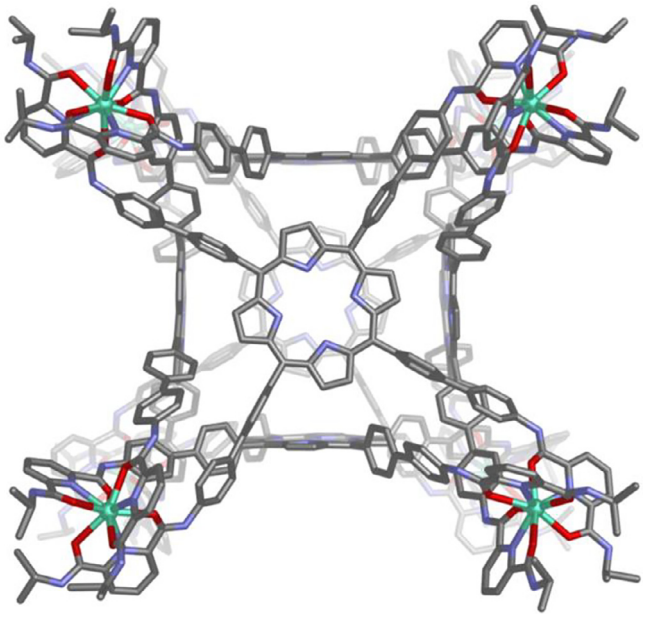

Fig. 30. Single crystal X-ray structure of a face-capped Ln_8L_6 cube (**71**) synthesized by Sun and coworkers [81].

a linear relationship between luminescence and 5-HIAA concentration, with sensitivity on the nanomolar scale, allowing for potential applications detecting tumor markers in biological samples.

Selective sensing of Mg(II) ions by a Ce_2L_3 helicate generated with three equivalents of ligand **70** (Fig. 29) has also been reported [36]. Single crystal X-ray diffraction data of the complex indicated the three β-diketone moieties on the ligands coalesced in the center of the helicate complex to form an octahedral binding site, capable of binding small metal ions (~0.7 Å radius.) Coordination of alkali and alkaline earth metal ions within this central site was investigated. An 8-fold increase in luminescence was observed with Mg(II), whilst all other species investigated (Li(I), Na(I), K(I), Ca(II) and Ba(II)) resulted in minimal luminescence changes. Competition experiments between Mg(II) and other metals determined that Mg(II) bound the strongest and could not be displaced by any of the other metal ions investigated. Binding with comparably sized transition metal ions (Fe(III), Cu(II) and Zn(II)) was also observed but resulted in luminescence quenching.

Fluoride sensing has also be investigated using a nitrate-templated tetranuclear circular helicate [118]. In this system, fluoride ions replaced non-coordinated nitrate counterions in the parent structure. Fluoride ions were favored over the nitrate ions as they formed hydrogen bonds with N—H moieties within malonohydrazone binding sites. Upon coordination of these fluoride ions an increase in the optical rotation of the architecture was observed *via* circular dichroism, alongside enhancing near-IR luminescence of Nd(III). The luminescence enhancement was attributed to a reduction of non-radiative decay with the Nd(III) transitions, while the increased optical rotation may be due to helicate aggregation.

The luminescence response of a large Yb_8(**47**)$_6$ cubic structure (**71**; Fig. 30) to a range of polyaromatic hydrocarbons (PAHs) has also been reported [81]. In the presence of small PAHs (naphthalene, anthracene and phenanthroline) and very large PAHs (rubrene and tetraphenylethylene) (Fig. 31), no change in luminescence is reported for the cubic structure. However, when PAHs of intermediate size (perylene, 1,12-benzoperylene and coronene) are introduced to a solution of **61**, a decrease in the quantum yield and luminescence lifetimes is observed. ^{1}H NMR and mass spectrometry experiments support encapsulation of these guest molecules within **61** and provided an explanation for the size-dependent sensing observed.

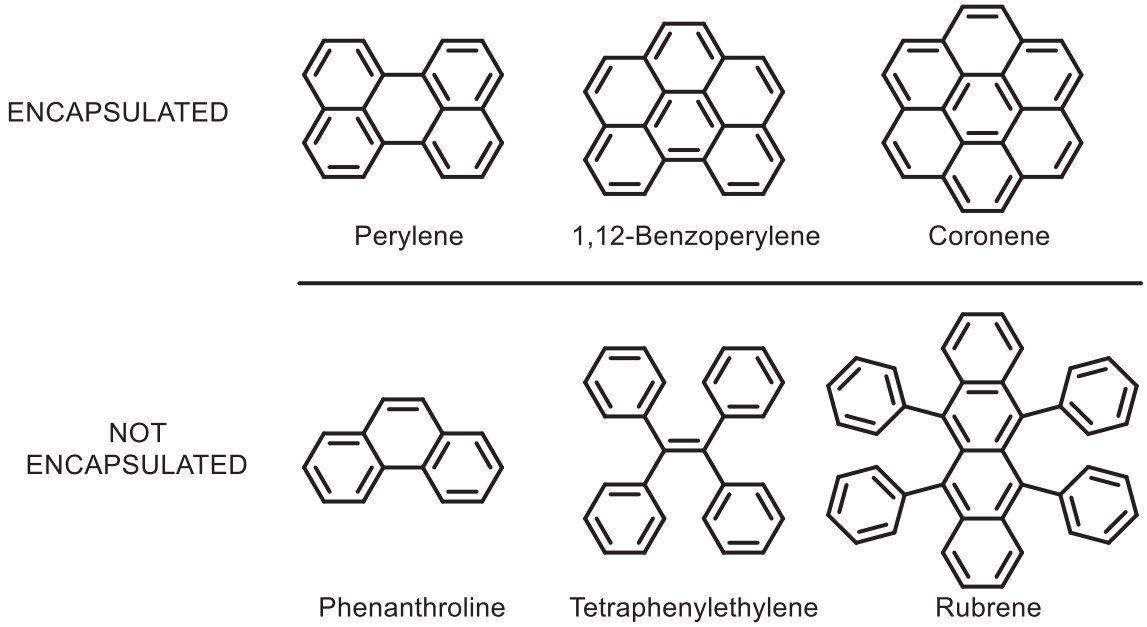

Fig. 31. Structure of polyaromatic hydrocarbons (PAHs) encapsulated within the Ln_8L_6 architecture (**71**) synthesized by Sun and coworkers [81].

In a bid to improve the luminescence properties of supramolecular lanthanide architectures, and thereby increase their utility as sensors, Sun and coworkers have synthesized metal–organic structures incorporating ligands capable of undergoing intraligand charge transfer (ILCT). ILCT sensitization of lanthanide ions can give rise to increased quantum yields, and has previously been studied in mononuclear complexes in great detail [119]. Ligands can exhibit charge transfer when electron donating and electron accepting moieties are bridged *via* π-conjugation as in **72** (Fig. 32). Sun and coworkers achieved ILCT in a multinuclear Eu_4L_4 architecture using a C_3-symmetric triazine linker with oxazoline-picolinamide binding sites (**72**) [35]. Absorption of light by benzamide moieties within the linker resulted in locally excited environments, which rapidly converted into excited ILCT states. Characteristic Eu(III) emission peaks were detected, confirming energy transfer from the excited ILCT state to the lanthanide ions. The Ln_4**72**$_4$ architecture exhibited selective luminescence quenching in the presence of iodide anions. Hydrogen bonding between the ligands and the iodide ions was observed and resulted in the blocking of the architectures pores. The decrease in luminescence was attributed to a combination of static and dynamic quenching processes. Further studies indicated a sevenfold reduction of the lifetime of the architectures' excited state, and a less efficient conversion from a locally excited state to the excited ILCT state. Conversely, the addition of transition metal cations resulted in luminescence enhancements of Eu_4**72**$_4$, with Cu(II) ions causing the largest enhancement. Cation-π interactions with the central triazine moiety increased luminescent lifetimes and increased the efficiency of local excited state to excited ILCT state conversion [120].

4.3. Separation

A key challenge surrounding the use of lanthanides is the current method of purification. Industrial separation relies upon liquid–liquid extraction focusing on mononuclear species and consumes vast amounts of solvents. Developing multitopic ligands, capable of lanthanide binding, may lead to more effective separation of trivalent lanthanide ions.

Using tritopic dipicolinamide-based ligands (**73**; Fig. 33), Sun and coworkers studied the formation of Ln_4L_4 architecture **74** to assess the effectiveness of separation of different lanthanide ions

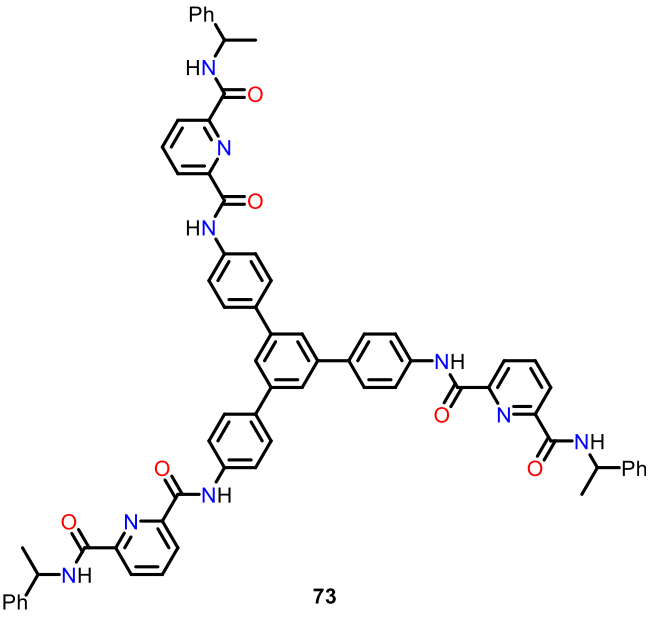

73

Fig. 33. Structure of ligand **73** used in the study of lanthanide separation *via* the formation of Ln_4**73**$_4$ tetrahedra (**74**), synthesized by Sun and coworkers [82].

and common impurities found in ores [82]. Common impurities found in lanthanide containing ores (such as Ca(II) and Cd(II)) were capable of forming M_4(**73**)$_4$ tetrahedra in isolation, but Ln_4L_4 architectures were formed with 100 % selectivity in 1:1 M:Ln ratios (where M = Ca(II)or Cd(II)) 100 % selectivity was also reported between certain lanthanide pairs, which were multiple atomic numbers apart, with smaller ions being favorably selected. Lanthanide pairs comprised of neighboring atoms such as La(III): Ce(III) or Ce(III): Nd(III) did not exhibit 100 % selectivity, varying between 80 and 90 %. Considering the La(III): Ce(III) solution, the majority of architectures formed were Ce_4(**73**)$_4$ tetrahedra, with a limited amount of heterometallic La_nCe_{4-n}(**73**)$_4$ tetrahedra as 89.3 % of the lanthanide ions in the sample were cerium(III). When compared to a C_2-symmetric ligand featuring the same binding moieties as the tritopic ligand, the larger ion formed the homometallic species in higher yields (Fig. 34).

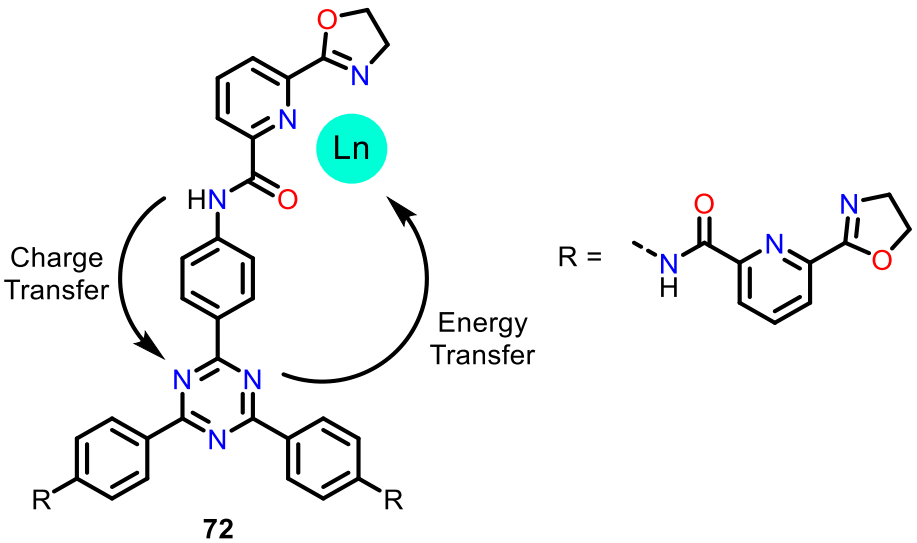

72

Fig. 32. Mechanism of ILCT sensitization of lanthanide luminescence with **72**, *via* charge transfer from a benzamide moiety to the central triazine. Energy is then transferred to the lanthanide ion where it is lost *via* radiative emission [35,63].

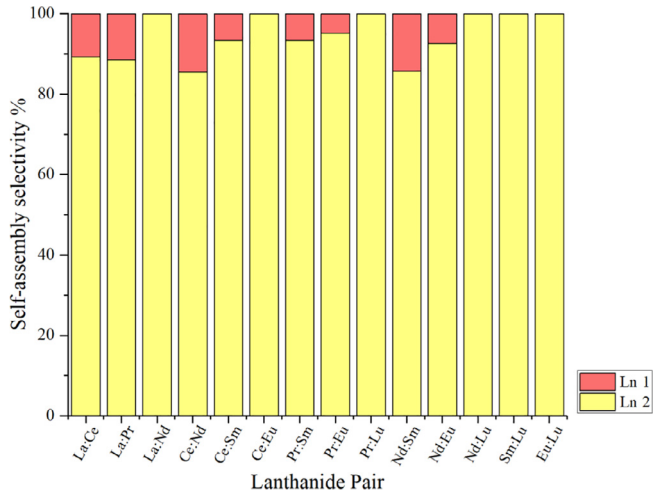

Fig. 34. Self-assembly selectivity between lanthanide ions in 1:1:1 stoichiometry (Ln 1: Ln 2: 7**3**).

It was hypothesized that liquid–liquid extraction could allow facile extraction of selected Ln(III) metals incorporated within Ln_4L_4 architectures from unbound contaminant ions. However, modification of the ligand with flexible alkyl groups to promote Ln_4L_4 stability in non-polar solvents negatively impacted the metal ions selectivity of the complexes. This indicates that an alternative approach to liquid–liquid extraction may be required if this methodology is to be successfully utilized.

4.4. Imaging

Building on promising initial results using lanthanide supramolecular complexes in sensing applications a number of bioimaging studies have also been undertaken. These early studies have sought to establish the stability of lanthanide complexes within aqueous environments, and the non-toxic nature of these probes.

In 2007 Bünzli and coworkers reported [21] the interaction of a water -soluble Eu_2(**75**)$_3$ helicate (**76**) with HeLa cells (Fig. 35). Suitable water-solubility for this complex was obtained by appending PEG chains to the ligand. The resulting helicate was shown to have good thermodynamic stability in pH 7.4 buffered solution and displayed metal centered luminescence and long lifetimes consistent with exclusion of water molecules from the europium(III) inner coordination sphere. Following incubation of **76** with HeLa cells, luminescence imaging clearly indicated that the complex had permeated the cells and stained the cytoplasm in a concentration dependent manner.

Quantification of helicate **76** uptake in cells incubated at 4 and 37 °C showed little difference in luminosity, indicating an active uptake mechanism is likely to be operative. While studies comparing cell proliferation and viability in the presence and absence of the helicate showed no significant differences up to 500 μM **76** concentration, confirming the potential of these systems for cell imaging.

Subsequent work by the same authors confirmed that increasing the PEG chain length to a hexakis(oxyethylene) moiety did not alter cellular uptake [22], with Eu(III) helicates permeating the cytoplasm *via* an endocytotic pathway. Once internalized leakage of the complex was found to be negligible over extended periods, and no evidence for metal–ligand dissociation was observed, even at the low intracellular concentrations of 0.28 μM reported. The complexes reported in this study again showed no appreciable cytotoxicity over 24 h of incubation at up to 500 μM concentrations. Taken together these results indicate the significant promise of these complexes for cellular imaging.

More recently Chen, Li, Sun and coworkers reported the synthesis of a family of anionic Ln_8(**77**)$_{12}$ (where Ln = Gd(III)) cubic complexes displaying potential as magnetic imaging contrast reagents (Fig. 36 [83]. As with the previous studies, the aqueous stability of these architectures is essential for realization of their desirable properties. The water stability is derived from the use of a previously unreported bis-tridentate tetrazolate chelating group (Fig. 15), with the stability of the complex attributed to both the chelate effect and the electrostatic interactions between the deprotonated ligand and the cationic metal ion. Meanwhile, functionalization of the parent ligand with a PEG chain imparts water solubility. Following structural characterization, the authors investigated the photophysical properties of the Ln_8(**77**)$_{12}$ architectures generated with Eu(III), Tb(III) and Gd(III). For complexes generated with **77**, quantum yields in water were reported as 5.5 % (Eu_8(**77**)$_{12}$) and 8.2 % (Tb_8(**77**)$_{12}$), while values of 76.3 % and 76.8 %, respectively, were reported in DMSO. These remarkable quantum yields were attributed to a combination of factors including the fully conjugated nature of the ligand, the rigid nature of the multinuclear architecture, the long lifetimes of the triplet states and the saturated coordination sphere of the metal ions (the number of inner sphere coordinated water molecules, q = 0.09 ± 0.5 Eu_8L_{12} in CH_3OH and CD_3OD). The stability of complexes incorporating **78** and **79** in aqueous and saline solutions was monitored

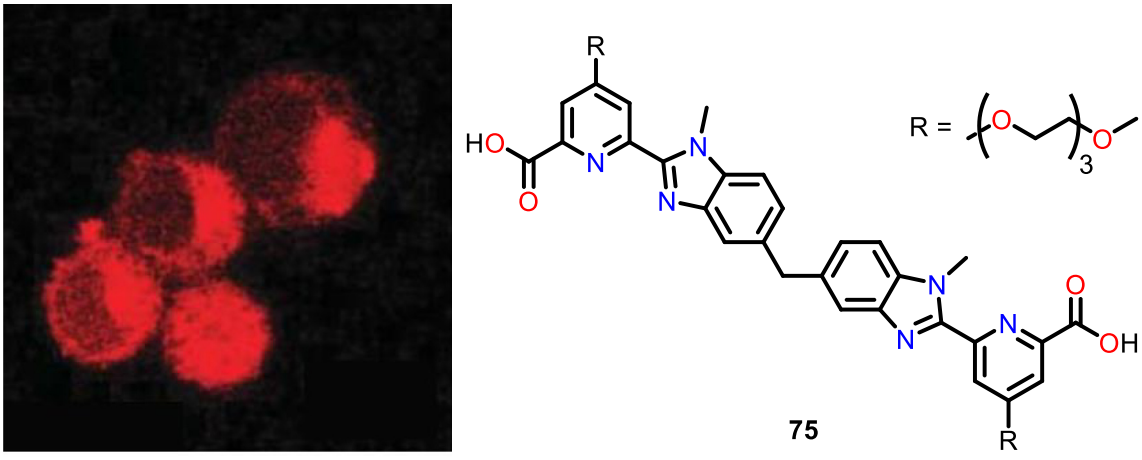

Fig. 35. Bimetallic triple-stranded stranded helicates (Eu_2(**75**)$_3$) encapsulated inside HeLa cells, incubated for 24 h at a concentration of 500 μM, taken from [21].

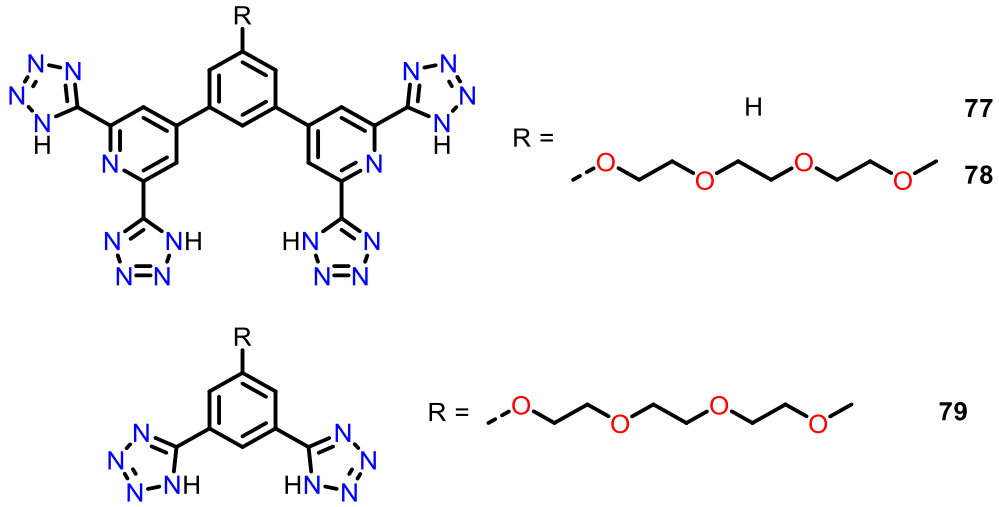

Fig. 36. Three ligands investigated for spectroscopic imaging ability (**77** and **78**) and as potential MRI contrast agents when complexed with Gd(III) (**78** and **79**) [83].

following dilution of DMSO solutions. Mass spectrometry and luminescence studies indicated excellent stability down to 10^{-6} M concentration over the course of 36 h. Inspired by these results, the authors evaluated the potential of Gd_8(**78**)$_{12}$ and mixed Gd/Eu cubic structures as MRI contrast agents. The Gd_8(**78**)$_{12}$ complex displayed extremely high longitudinal relaxivity of 400.53 $mM^{-1}s^{-1}$ and showed much longer retention in tumor sites than commercial reagents with no decrease after 24 h. Cytotoxicity studies revealed both the Gd_8(**78**)$_{12}$ and mixed Gd/Eu complexes displayed lower cytotoxicity than cisplatin in HK-2 cells indicating the potential application of these complexes as dual imaging agents.

The ability of three helical Fe(III)-Gd(III) species to act as effective MRI contrast agents has also been investigated [99]. The longest of the three species ($FeGd_2$**59**$_3$) exhibited the highest T_1 relaxivity of the three studied (R_1 = 42 mM^{-1} s^{-1} at 1.5 T), this was hypothesized to be due to slower molecular tumbling of this complex in comparison to the shorter structures investigated.

Collectively, these initial studies highlight the potential of lanthanide supramolecular architectures for imaging applications but the sparsity of literature in this area is indicative of the challenges the field faces, particularly with regard to generation of water-stable luminescent architectures.

4.5. Magnetism

In addition to the potential application of lanthanide architectures as outlined above, the magnetic properties of architectures incorporating lanthanide ions are of great interest due to the large spin quantum numbers and magnetic moments of many of the metal ions [121]. Research into lanthanide complexes focuses on two major applications: cryogenic magnetic refrigerants [122] and single molecule magnets [123]. To the best of our knowledge, magnetic studies of supramolecular lanthanide architectures have been limited, focusing on circular helicates [60,124] and octahedral architectures [40].

The magnetocaloric effect (MCE) is the phenomena behind cryogenic magnetic refrigeration [125]. MCE causes changes in temperature and magnetic entropy of a sample, by altering an applied magnetic field. Magnetic entropy change, ΔS_M, is used as a measure of a systems magnetocaloric effect with lower values being desired. Currently systems based on first row transition metal complexes are utilized in commercial applications as the low price and abundance of the metal ions was initially favored over the metal ion performance. However, it is widely accepted that the strong coupling present between 3d-metal centers results in larger ΔS_M values, meaning that weakly interacting lanthanide ions could be more effective. A majority of recent research in this area has focused on Gd(III) complexes, due to the ion having the largest spin quantum number, S = 7/2, and minimal anisotropy. Structures tend to contain a large amount of Gd(III) ions, although lanthanide clusters are more prominent than supramolecular architectures.

Single molecule magnets (SMMs) are characterized by an ability to maintain magnetization over an extended period of time, without the application of an external magnetic field [16]. A majority of SMMs require helium cooling, allowing for magnetization retention over multiple years. Recent examples have retained magnetization under liquid nitrogen cooling, although magnetization diminishes over a few hours [126]. Initial research into SMMs focused on transition metal complexes, mainly containing Mn(II) ions, but these are outperformed by more recent lanthanide complexes [127]. Current research is mainly focused on terbium(III) and dysprosium(III)-based complexes. Both ions possess large magnetic anisotropy and sizeable energy gaps between their respective ground and excited magnetic energy levels, m_J. Dysprosium(III) based complexes are more prevalent in the literature, due to the Dy(III) ion possessing an odd number of f-electrons (nine), resulting in a bistable ground state independent of ligand field effects [128].

Konar and coworkers synthesized a Gd_4(**19**)$_4$ circular helicate analogous to a previously reported architecture [38,124]. Magnetic studies obtained gravimetric magnetic entropy values ($-\Delta S_m$ = 24.4 $Jkg^{-1}K^{-1}$) comparable to previously reported gadolinium complexes [125]. Observed values were slightly lower than calculated values due to antiferromagnetic interactions between neighboring Gd(III) ions. Two Dy_4L_4 circular helicates were reported, one analogous to the Gd_4L_4, with the second species a having distorted nitrate ion centrally, binding to all four ions, resulting in slightly different coordination environments. Both of these structures exhibited SMM-like behavior, although neither sample was competitive with known SMMs [129] due to low effective energy barriers, resulting in poor retention of magnetization.

Tang and coworkers reported two iterations of a Gd_6L_6 circular helicate, comprised of ligands using propylene-bridged malonohydrazone binding sites [60]. The architectures varied by counterion used, and the coordinated solvent molecules, $Gd_6L_6.(CF_3SO_3)_6(DMF)_{12}$ and $Gd_6L_6.(ClO_4)_6(DMF)_{10}(H_2O)_2$. The structural variations resulted in slight differences in calculated and measured entropy

changes. Experimentally determined gravimetric magnetic entropy values for the two structures were 40 % lower than for the previously reported Gd_4L_4 circular helicate. The experimental values were also lowered than the calculated values, believed to be due to the large ligands, and weak antiferromagnetic interactions within the system. Dysprosium(III) analogues of the hexanuclear circular helicate had miniscule energy barriers, suggesting magnetization could not be retained.

Multi-heteronuclear dysprosium squares utilizing **61** reported by Tang and coworkers [102] exhibited SMM behavior, however the energy barrier to magnetization is low (below 12 K) compared to literature values indicating significant redesign of these complexes is required if impactful contributions are to be made in the SMM field. Dodecanuclear dysprosium octahedral complexes ($Ln_{12}L_{12}$) synthesized from butylene-bridged malonohydrazone binding sites were investigated for their magnetic properties. The $Ln_{12}L_{12}$ complexes displayed typical SMM behavior, with one complex exhibiting SMM behavior in a 0 Oe dc field. The coordination geometries of the dysprosium ions resulted in large variations in this regard [40].

The paucity of literature examples of reported gadolinium(III) and dysprosium(III) multinuclear lanthanide architectures, especially tetra- or hexanuclear circular helicates, have limited development towards potential applications of SMMs or magnetic refrigerants. Further research into this field may elucidate alternative architectures with improved magnetic characteristics.

5. Conclusions and outlook

The number and complexity of polynuclear lanthanide organic cages is beginning to grow rapidly, and many opportunities exist for these structures in applications ranging from catalysis to separations and biological imaging. Initial studies with low nuclearity helicates demonstrated many ligand design criteria which have informed the development of larger structures incorporating increased numbers of metal ions and ligands. As with transition metal organic cages the rigidity of the ligand and the offset of the chelating groups within the ligand directs the architecture obtained. Unlike transition metal ions, however, the larger coordination numbers of lanthanide ions introduces variability in the number of ligands coordinated to the metal ion, typically varying from two to four, and introduces the possibility for inclusion of ancillary components in a supramolecular structure. In order to be robust to hydrolysis good ligand wrapping is required whereby the coordinated ligands exclude any water molecules from the lanthanide metal coordination sphere, this can be promoted by introduction of bulky, organic substituents on the termini of the ligands. Displacement of ligands through preferential binding of water or solvent molecules within the metal coordination sphere of transition metal complexes is comparatively rare. The choice of ligand donor atoms is another important consideration when designing LOP, with hard N and O atoms being incorporated through a variety of a chelating moieties. Recent publications have shown oxazoline converted dipicolinic amides and novel 2,6-pyridine bitetrazolate moieties have improved aqueous stability over previously reported coordination motifs, whereas the triazole-pyridine-triazole moiety has superior photoluminescence properties. In common with transition metal based self-assembly judicious choice and placement of PEG chains or chiral functionalities on the ligand imparts water solubility and directs chirality without significant structural implications.

Development of the field should look to continued improvement in the aqueous stability of these complexes given their clear potential in biological imaging applications. Further development and testing of chelating moieties alongside incorporation of water solubilizing groups is a clear strategy to achieve this goal. Incorporation of the recently published 2,6-pyridine bitetrazolate chelating group into different ligand backbones including a tritopic ligand would be an excellent starting point. This would allow any potential influence of the ligand coordination vector to be identified revealing the generality of the 2,6-pyridine bitetrazolate moiety in formation of multinuclear water-stable lanthanide complexes.

Further development of water-soluble constructs as drug delivery vehicles is also targeted, with luminescence sensing capabilities providing a potential route to theranostic treatment whereby information on a diagnosis is obtained at the same time as delivery of a drug molecule. At a more fundamental level the development of LOP capable of delivering a payload whilst emitting a spatial and temporal signal is also appealing as a research tool.

More generally, novel ligands that support formation of larger complexes should be sought. Recent results demonstrating formation of Ln_8L_{12} cubic structures and $Ln_{10}L_{15}$ complexes are promising but the current diversity of supramolecular lanthanide complexes lies well behind that of their transition metal counterparts limiting their applications. Further investigation of the catalytic potential of lanthanide cages should also be undertaken. The higher overall charge of many lanthanide cages versus comparable transition metal cages (12 + versus 8 +) indicates they may be good candidates for supporting catalytic processes in which the charge state of the substrate changes [130]. For the current systems reported to promote catalysis (Section 4.1) the role of the metal ion, and the overall charge of the cage is poorly defined with the cavity size and hydrogen bonding capability of the ligand being cited as the key drivers for the observed transformations.

The potential magnetic opportunities of lanthanide cages have also been highlighted with initial reports of circular helicates and then an octahedral cage indicating promising behavior. Synthesis and characterization of more dysprosium, and gadolinium polyhedra should be undertaken to enable identification of the structural properties to be optimized to achieve the best magnetic properties. Given the limited examples in this area, a broad range of structures should be considered before refining the experimental space.

More detailed investigations into the role of the lanthanide ions within the cages will undoubtedly enable design of new systems capable of undertaking alternative catalytic processes, displaying interesting magnetic properties, and acting as traceable delivery vehicles as well as contributing to as yet unforeseen applications.

Data availability

No data was used for the research described in the article.

Declaration of Competing Interest

The authors declare that they have no known competing financial interests or personal relationships that could have appeared to influence the work reported in this paper.

Acknowledgements

This research was supported by a Royal Society University Research Fellowship (IAR; URF\R1\180414), the Engineering and Physical Sciences Research Council and the Department of Chemistry at the University of Manchester through the award of a DTG studentship.

References:

[1] J.M. Lehn, A. Rigault, J. Siegel, J. Harrowfield, B. Chevrier, D. Moras, Proc. Natl. Acad. Sci. U. S. A. 84 (1987) 2565–2569.

[2] P. Mal, B. Breiner, K. Rissanen, J.R. Nitschke, Science 324 (2009) 1697–1699.
[3] D.L. Caulder, R.E. Powers, T.N. Parac, K.N. Raymond, Angew. Chem. Int. Ed. 37 (1998) 1840–1843.
[4] P. Mal, D. Schultz, K. Beyeh, K. Rissanen, J.R. Nitschke, Angew. Chem. Int. Ed. 47 (2008) 8297–8301.
[5] W. Meng, B. Breiner, K. Rissanen, J.D. Thoburn, J.K. Clegg, J.R. Nitschke, Angew. Chem. Int. Ed. 50 (2011) 3479–3483.
[6] S. Roche, C. Haslam, H. Adams, S.L. Heath, J.A. Thomas, Chem. Commun. (1998) 1681–1682.
[7] S.M. Jansze, D. Ortiz, F. Fadaei Tirani, R. Scopelliti, L. Menin, K. Severin, Chem. Commun. 54 (2018) 9529–9532.
[8] M.M.J. Smulders, A. Jiménez, J.R. Nitschke, Angew. Chem. Int. Ed. 51 (2012) 6681–6685.
[9] Q.F. Sun, J. Iwasa, D. Ogawa, Y. Ishido, S. Sato, T. Ozeki, Y. Sei, K. Yamaguchi, M. Fujita, Science 328 (2010) 1144–1147.
[10] D. Fujita, Y. Ueda, S. Sato, H. Yokoyama, N. Mizuno, T. Kumasaka, M. Fujita, Chem 1 (2016) 91–101.
[11] D. Fujita, Y. Ueda, S. Sato, N. Mizuno, T. Kumasaka, M. Fujita, Nature 540 (2016) 563–566.
[12] R.C. Johnson, J. Chem. Educ. 42 (1965) 147–148.
[13] V. Bhalla, Resonance 23 (2018) 277–290.
[14] J.M. Lehn, Angew. Chem. Int. Ed. 27 (1988) 89–112.
[15] X.-Z. Li, C.-B. Tian, Q.-F. Sun, Chem. Rev. 122 (2022) 6374–6458.
[16] J.-C.-G. Bünzli, J. Coord. Chem. 67 (2014) 3706–3733.
[17] R.D. Shannon, Acta Crystallogr., A 32 (1976) 751–767.
[18] C. Piguet, J.-C.-G. Bünzli, G. Bernardinelli, G. Hopfgartner, A.F. Williams, J. Alloys Compd. 225 (1995) 324–330.
[19] E.M. Fatila, A.C. Maahs, E.E. Hetherington, B.J. Cooper, R.E. Cooper, N.N. Daanen, M. Jennings, S.E. Skrabalak, K.E. Preuss, Dalton Trans. 47 (2018) 16232–16241.
[20] E. Soini, H. Kojola, Clin. Chem. 29 (1983) 65–68.
[21] C.D.B. Vandevyver, A.-S. Chauvin, S. Comby, J.-C.-G. Bünzli, Chem. Commun. (2007) 1716–1718.
[22] E. Deiters, B. Song, A.-S. Chauvin, C.D.B. Vandevyver, J.-C.-G. Bünzli, New J. Chem. 32 (2008) 1140–1152.
[23] J.-C.-G. Bünzli, A.-S. Chauvin, C.D.B. Vandevyver, S. Bo, S. Comby, Ann. N. Y. Acad. Sci. 1130 (2008) 97–105.
[24] S.V. Eliseeva, B. Song, C.D.B. Vandevyver, A.S. Chauvin, J.B. Wacker, J.-C.-G. Bünzli, New J. Chem. 34 (2010) 2915–2921.
[25] Y.-G. Huang, F.-L. Jiang, M.-C. Hong, Coord. Chem. Rev. 253 (2009) 2814–2834.
[26] X.Y. Zheng, X.J. Kong, Z. Zheng, L.S. Long, L.S. Zheng, Acc. Chem. Res. 51 (2018) 517–525.
[27] R. Sessoli, A.K. Powell, Coord. Chem. Rev. 253 (2009) 2328–2341.
[28] C. Bai, B. Liu, H.-M. Hu, J.-D. Li, X. Wang, G. Xue, Acta Crystallogr., C 75 (2019) 422–432.
[29] K. Liu, X. Zhang, X. Meng, W. Shi, P. Cheng, A.K. Powell, Chem. Soc. Rev. 45 (2016) 2423–2439.
[30] D.A. Leigh, L. Pirvu, F. Schaufelberger, J. Am. Chem. Soc. 141 (2019) 6054–6059.
[31] G. Zhang, G. Gil-Ramírez, A. Markevicius, C. Browne, I.J. Vitorica-Yrezabal, D. A. Leigh, J. Am. Chem. Soc. 137 (2015) 10437–10442.
[32] C. Piguet, A.F. Williams, G. Bernardinelli, Angew. Chem. Int. Ed. 31 (1992) 1622–1624.
[33] M. Elhabiri, R. Scopelliti, J.-C.-G. Bünzli, C. Piguet, Chem. Commun. (1998) 2347–2348.
[34] C. Lincheneau, C. Destribats, D.E. Barry, J.A. Kitchen, R.D. Peacock, T. Gunnlaugsson, Dalton Trans. 40 (2011) 12056–12059.
[35] C.-L. Liu, R.-L. Zhang, C.-S. Lin, L.-P. Zhou, L.-X. Cai, J.-T. Kong, S.-Q. Yang, K.-L. Han, Q.-F. Sun, J. Am. Chem. Soc. 139 (2017) 12474–12479.
[36] X. Zhu, C. He, D. Dong, Y. Liu, C. Duan, Dalton Trans. 39 (2010) 10051–10055.
[37] J. Zhang, C. He, C. Duan, Inorg. Chem. Commun. 49 (2014) 140–142.
[38] A. Malviya, H.S. Jena, A.K. Mondal, S. Konar, Eur. J. Inorg. Chem. 2015 (2015) 2901–2907.
[39] B. Wang, Z. Zang, H. Wang, W. Dou, X. Tang, W. Liu, Y. Shao, J. Ma, Y. Li, J. Zhou, Angew. Chem. Int. Ed. 52 (2013) 3756–3759.
[40] Y. Zhang, B. Ali, J. Wu, M. Guo, Y. Yu, Z. Liu, J. Tang, Inorg. Chem. 58 (2019) 3167–3174.
[41] Z. Zhang, Y. Zhou, H. Li, T. Gao, P. Yan, Dalton Trans. 48 (2019) 4026–4034.
[42] T.Y. Bing, T. Kawai, J. Yuasa, J. Am. Chem. Soc. 140 (2018) 3683–3689.
[43] L.-L. Yan, C.-H. Tan, G.-L. Zhang, L.-P. Zhou, J.-C. Bünzli, Q.-F. Sun, J. Am. Chem. Soc. 137 (2015) 8550–8555.
[44] M. Borkovec, J. Hamáček, C. Piguet, Dalton Trans. (2004) 4096–4105.
[45] J. Hamacek, M. Borkovec, C. Piguet, Dalton Trans. (2006) 1473–1490.
[46] C. Piguet, J.-C.G. Bünzli, Self-Assembled Lanthanide Helicates: From Basic Thermodynamics to Applications, in: Handbook on the Physics and Chemistry of Rare Earths, Elsevier, 2010, pp. 301-553.
[47] J. Hamacek, Self-Assembly Principles of Helicates, in: G. Maayan, M. Albrecht (Eds.), Metallofoldamers: Supramolecular Architectures From Helicates to Biomimetics, John Wiley & Sons Ltd, 2013, pp. 91–123.
[48] C. Piguet, Microscopic Thermodynamic Descriptors for Rationalizing Lanthanide Complexation Processes, in: J.-.-C.-G. Bünzli, V.K. Pecharsky (Eds.), Handbook on the Physics and Chemistry of Rare Earths, Elsevier, 2015, pp. 209–271.
[49] J. Hamacek, S. Blanc, M. Elhabiri, E. Leize, A. Van Dorsselaer, C. Piguet, A.-M. Albrecht-Gary, J. Am. Chem. Soc. 125 (2003) 1541–1550.
[50] N. André, T.B. Jensen, R. Scopelliti, D. Imbert, M. Elhabiri, G. Hopfgartner, C. Piguet, J.C.G. Bünzli, Inorg. Chem. 43 (2004) 515–529.
[51] O. Kotova, S. Comby, K. Pandurangan, F. Stomeo, J.E. O'Brien, M. Feeney, R.D. Peacock, C.P. McCoy, T. Gunnlaugsson, Dalton Trans. 47 (2018) 12308–12317.
[52] T. Zhang, G.-L. Zhang, L.-P. Zhou, X.-Q. Guo, Q.-F. Sun, Tetrahedron Asymmetry 28 (2017) 550–554.
[53] S. Floquet, N. Ouali, B. Bocquet, G. Bernardinelli, D. Imbert, J.-C.-G. Bünzli, G. Hopfgartner, C. Piguet, Chem. - A Eur. J. 9 (2003) 1860–1875.
[54] K. Zeckert, J. Hamacek, J.M. Śenegas, N. Dalla-Favera, S. Floquet, G. Bernardinelli, C. Piguet, Angew. Chem. Int. Ed. 44 (2005) 7954–7958.
[55] H. Li, T. Gao, P. Yan, Y. Zhou, Y. Yao, Z. Cheng, Dalton Trans. 49 (2020) 3312–3320.
[56] J. Shi, Y. Hou, W. Chu, X. Shi, H. Gu, B. Wang, Z. Sun, Inorg. Chem. 52 (2013) 5013–5022.
[57] Y. Zhou, Y. Yao, Z. Cheng, T. Gao, H. Li, P. Yan, Inorg. Chem. 59 (2020) 12850–12857.
[58] Z. Yao, Y. Zhou, T. Gao, P. Yan, H. Li, RSC Adv. 11 (2021) 10524–10531.
[59] J.M. Senegas, S. Koeller, G. Bernardinelli, C. Piguet, Chem. Commun. (2005) 2235–2237.
[60] J. Lu, V. Montigaud, O. Cador, J. Wu, L. Zhao, X.L. Li, M. Guo, B. Le Guennic, J. Tang, Inorg. Chem. 58 (2019) 11903–111901.
[61] T.K. Ronson, H. Adams, L.P. Harding, S.J.A. Pope, D. Sykes, S. Faulkner, M.D. Ward, Dalton Trans. (2007) 1006–1022.
[62] B. Wang, B. Ma, Z. Wei, H. Yang, M. Wang, W. Yin, H. Gao, W. Liu, Inorg. Chem. 60 (2021) 2764–2770.
[63] X.-Z. Li, L.-P. Zhou, L.-L. Yan, D.-Q. Yuan, C.-S. Lin, Q.-F. Sun, J. Am. Chem. Soc. 139 (2017) 8237–8244.
[64] J. Hamacek, G. Bernardinelli, Y. Filinchuk, Eur. J. Inorg. Chem. (2008) 3419–3422.
[65] G. Canard, S. Koeller, G. Bernardinelli, C. Piguet, J. Am. Chem. Soc. 130 (2008) 1025–1040.
[66] J. Hamacek, C. Besnard, T. Penhouet, P.-Y. Morgantini, Chem. - A Eur. J. 17 (2011) 6753–6764.
[67] B. El Aroussi, L. Guénée, P. Pal, J. Hamacek, Inorg. Chem. 50 (2011) 8588–8597.
[68] J. Hamacek, D. Poggiali, S. Zebret, B.E. Aroussi, M.W. Schneider, M. Mastalerz, Chem. Commun. 48 (2012) 1281–1283.
[69] A. Vuillamy, S. Zebret, C. Besnard, V. Placide, S. Petoud, J. Hamacek, Inorg. Chem. 56 (2017) 2742–2749.
[70] J. Hamacek, A. Vuillamy, L. Peterhans, A. Homberg, D. Poggiali, M.W. Schneider, M. Mastalerz, New J. Chem., 42 (2018) 7803-7803.
[71] S.-Y. Wu, X.-Q. Guo, L.-P. Zhou, Q.-F. Sun, Inorg. Chem. 58 (2019) 7091–7098.
[72] S.J. Hu, X.Q. Guo, L.P. Zhou, L.X. Cai, Q.F. Sun, Chinese J. Chem. 37 (2019) 657–662.
[73] S.-J. Hu, X.-Q. Guo, L.-P. Zhou, D.-N. Yan, P.-M. Cheng, L.-X. Cai, X.-Z. Li, Q.-F. Sun, J. Am. Chem. Soc. 144 (2022) 4244–4253.
[74] Y. Zhou, H. Li, T. Zhu, T. Gao, P. Yan, J. Am. Chem. Soc. 141 (2019) 19634–19643.
[75] Y. Jiao, C. He, C.-Y. Duan, Inorg, Chem. Commun. 39 (2014) 147–150.
[76] C.-L. Liu, L.-P. Zhou, D. Tripathy, Q.-F. Sun, Chem. Commun. 53 (2017) 2459–2462.
[77] K.-H. Yim, C.-T. Yeung, M.R. Probert, W.T.K. Chan, L.E. Mackenzie, R. Pal, W.-T. Wong, G.-L. Law, Comm. Chem., 4 (2021) 116-116.
[78] C. Piguet, Chem. Commun. 46 (2010) 6209.
[79] C.-T. Yeung, K.-H. Yim, H.-Y. Wong, R. Pal, W.-S. Lo, S.-C. Yan, M. Yee-Man Wong, D. Yufit, D.E. Smiles, L.J. McCormick, S.J. Teat, D.K. Shuh, W.-T. Wong, G.-L. Law, Nat. Comm. 8 (2017) 1128.
[80] H. Ratni, J.J. Jodry, J. Lacour, E.P. Kündig, Organometallics 19 (2000) 3997–3999.
[81] X.-Z. Li, L. Zhou, S.-J. Hu, L.-X. Cai, X.-Q. Guo, Z. Wang, Q.-F. Sun, Chem. Commun. 56 (2020) 4416–4419.
[82] X.-Z. Li, L.-P. Zhou, L.-L. Yan, Y.-M. Dong, Z.-L. Bai, X.-Q. Sun, J. Diwu, S. Wang, J.-C. Bünzli, Q.F. Sun, Nat. Comm., 9 (2018) 547-547.
[83] Z. Wang, L. He, B. Liu, L.-P. Zhou, L.-X. Cai, S.-J. Hu, X.-Z. Li, Z. Li, T. Chen, X. Li, Q.-F. Sun, J. Am. Chem. Soc. 142 (2020) 16409–16419.
[84] S. Zebret, E. Vögele, T. Klumpler, J. Hamacek, Chem. - A Eur. J. 21 (2015) 6695–6699.
[85] X. Tang, D. Chu, W. Gong, Y. Cui, Y. Liu, Angew. Chem. Int. Ed. 60 (2021) 9099–9105.
[86] S. Torelli, S. Delahaye, A. Hauser, G. Bernardinelli, C. Piguet, Chem. - A Eur. J. 10 (2004) 3503–3516.
[87] G. Canard, C. Piguet, Inorg. Chem. 46 (2007) 3511–3522.
[88] T. Riis-Johannessen, N. Dupont, G. Canard, G. Bernardinelli, A. Hauser, C. Piguet, Dalton Trans. (2008) 3661–3677.
[89] C. Piguet, G. Hopfgartner, A.F. Williams, J.-C.-G. Bünzli, J. Chem. Soc., Chem. Commun. (1995) 491–493.
[90] C. Piguet, E. Rivara-Minten, Helv. Chim. Acta 78 (1995) 1541–1566.
[91] C. Piguet, E. Rivara-Minten, Helv. Chim. Acta 78 (1995) 1651–1672.
[92] C. Piguet, E. Rivara-Minten, G. Bernardinelli, J.-C.-G. Bünzli, G. Hopfgartner, J. Chem. Soc., Dalton Trans. (1997) 421–434.
[93] C. Edder, C. Piguet, J.-C.-G. Bünzli, G. Hopfgartner, Chem. - A Eur. J. 7 (2001) 3014–3024.
[94] M. Cantuel, G. Bernardinelli, D. Imbert, J.-C.-G. Bünzli, G. Hopfgartner, C. Piguet, J. Chem. Soc., Dalton Trans. (2002) 1929–1940.
[95] C. Piguet, J.-C.-G. Bünzli, G. Bernardinelli, G. Hopfgartner, S. Petoud, O. Schaad, J. Am. Chem. Soc. 118 (1996) 6681–6697.

[96] C. Edder, C. Piguet, J.-C.-G. Bünzli, G. Hopfgartner, Dalton Trans. (1997) 4657–4664.
[97] T. Riis-Johannessen, G. Bemardinelli, Y. Fillnchuk, S. Clifford, N.D. Favera, C. Piguet, Inorg. Chem. 48 (2009) 5512–5525.
[98] M. Cantuel, F. Gumy, J.-C.-G. Bünzli, C. Piguet, Dalton Trans. (2006) 2647–2660.
[99] V.C. Pierre, M. Botta, S. Aime, K.N. Raymond, J. Am. Chem. Soc. 128 (2006) 9272–9273.
[100] D. Guo, C.-Y. Duan, F. Lu, Y. Hasegawa, Q.-J. Meng, S. Yanagida, Chem. Commun. (2004) 1486–1487.
[101] J. Wu, L. Zhao, M. Guo, J. Tang, Chem. Commun 51 (2015) 17317–17320.
[102] J. Wu, L. Zhao, L. Zhang, X.-L. Li, M. Guo, J. Tang, Inorg. Chem. 55 (2016) 5514–5519.
[103] Z. Wang, L.-P. Zhou, T.-H. Zhao, L.-X. Cai, X.-Q. Guo, P.-F. Duan, Q.-F. Sun, Inorg. Chem. 57 (2018) 7982–7992.
[104] D. Yang, J.L. Greenfield, T.K. Ronson, L.K.S. Von Krbek, L. Yu, J.R. Nitschke, J. Am. Chem. Soc. 142 (2020) 19856–19861.
[105] W.D. Kohn, O.D. Monera, C.M. Kay, R.S. Hodges, J. Biol. Chem. 270 (1995) 25495–25506.
[106] M. Samiappan, S. Alasibi, R. Cohen-Luria, A. Shanzer, G. Ashkenasy, Chem. Commun. 48 (2012) 9577–9579.
[107] A.M. Webster, A.F.A. Peacock, Chem. Commun., 57 (2021) 6851-6851.
[108] L.N. Slope, O.J. Daubney, H. Campbell, S.A. White, A.F.A. Peacock, Angew. Chem. Int. Ed. 60 (2021) 24473–24477.
[109] E. Pidcock, G.R. Moore, J. Biol. Inorg. Chem. 6 (2001) 479–489.
[110] A. Kashiwada, K. Ishida, K. Matsuda, Bull. Chem. Soc. Jpn. 80 (2007) 2203–2207.
[111] M.R. Berwick, D.J. Lewis, A.W. Jones, R.A. Parslow, T.R. Dafforn, H.J. Cooper, J. Wilkie, Z. Pikramenou, M.M. Britton, A.F.A. Peacock, J. Am. Chem. Soc. 136 (2014) 1166–1169.
[112] M. Fujita, D. Oguro, M. Miyazawa, H. Oka, K. Yamaguchi, K. Ogura, Nature 378 (1995) 469–471.
[113] Y. Jiao, J. Wang, P. Wu, L. Zhao, C. He, J. Zhang, C. Duan, Chem. - A Eur. J. 20 (2014) 2224–2231.
[114] M. Yoshizawa, M. Tamura, M. Fujita, Science 312 (2006) 251–254.
[115] J. Zhang, C. He, C. Duan, Inorg, Chem. Commun. 54 (2015) 41–44.
[116] Y. Jiao, H.-Y. He, J.-Q. Yin, L. Zhou, C. He, C.-Y. Duan, Inorg, Chem. Comm. 73 (2016) 129–133.
[117] A.L. Agranovich, G.H. Anderson, M. Manji, B.D. Acker, W.C. Macdonald, W.J. Threlfall, J. Surg. Oncol. 47 (1991) 45–52.
[118] W. Chen, X. Tang, W. Dou, B. Wang, L. Guo, Z. Ju, W. Liu, Chem. - A Eur. J. 23 (2017) 9804–9811.
[119] A. D'Aléo, F. Pointillart, L. Ouahab, C. Andraud, O. Maury, Coord. Chem. Rev. 256 (2012) 1604–1620.
[120] A.S. Mahadevi, G.N. Sastry, Chem. Rev. 113 (2013) 2100–2138.
[121] L. Sorace, D. Gatteschi, Electronic Structure and Magnetic Properties of Lanthanide Molecular Complexes, in: R.A. Layfield, M. Murugesu (Eds.) Lanthanides and Actinides in Molecular Magnetism, Wiley-VCH Verlag GmbH & Co. KGaA, 2015.
[122] S.F. Kral, J.A. Barclay, Magnetic Refrigeration: A Large Cooling Power Cryogenic Refrigeration Technology, in: J.P. Kelley (Ed.), Applications of Cryogenic Technology, Applications of Cryogenic Technology, Springer, US, Boston, MA, 1991, pp. 27–41.
[123] N.T. Madhu, J.K. Tang, I.J. Hewitt, R. Clérac, W. Wernsdorfer, J.V. Slageren, C.E. Anson, A.K. Powell, ChemInform 37 (2006) 2864–2869.
[124] A.K. Mondal, H.S. Jena, A. Malviya, S. Konar, Inorg. Chem. 55 (2016) 5237–5244.
[125] J.L. Liu, Y.C. Chen, F.S. Guo, M.L. Tong, Coord. Chem. Rev. 281 (2014) 26–49.
[126] F.S. Guo, B.M. Day, Y.C. Chen, M.L. Tong, A. Mansikkamäki, R.A. Layfield, Science 362 (2018) 1400–1403.
[127] R. Sessoli, D. Gatteschi, H.L. Tsai, D.N. Hendrickson, A.R. Schake, S. Wang, J.B. Vincent, G. Christou, K. Folting, J. Am. Chem. Soc. 115 (1993) 1804–1816.
[128] J.D. Rinehart, J.R. Long, Chem. Sci. 2 (2011) 2078–2085.
[129] C.A.P. Goodwin, F. Ortu, D. Reta, N.F. Chilton, D.P. Mills, Nature 548 (2017) 439–442.
[130] M. Morimoto, S.M. Bierschenk, K.T. Xia, R.G. Bergman, K.N. Raymond, F.D. Toste, Nat. Catal. 3 (2020) 969–984.